이학석사학위논문

Nrd1 과 Nuclear exosome 그리고 RNA 중합효소 II
C-말단지역 간의 상호작용에 대한 Mpp6 의 조절작용 연구

Mpp6 regulates the interaction of Nrd1 with nuclear exosome and the C-terminal domain of RNA polymerase II

2015 년 2 월

서울대학교 대학원
생물물리 및 화학생물학과
김 규 민

Mpp6 regulates the interaction of Nrd1 with nuclear exosome and the C-terminal domain of RNA polymerase II

지도교수 이 준 호

이 논문을 이학석사학위논문으로 제출함

2015 년 2 월

서울대학교 대학원

생물물리 및 화학생물학과

김 규 민

김규민의 이학석사학위논문을 인준함

2014 년 12 월

위 원 장 석 영 재 (인)

부 위 원 장 이 준 호 (인)

위 원 김 민 규 (인)

Mpp6 regulates the interaction of Nrd1 with nuclear exosome and the C-terminal domain of RNA polymerase II

A dissertation submitted in partial fulfillment of the

requirement for the degree of

MASTER OF SCIENCE

to the faculty of the

Interdisciplinary Graduate Program in Biophysics and Chemical Biology

at

SEOUL NATIONAL UNIVERSITY

by

Kyumin KIM

Date Approved:

12/29/2014

ABSTRACT

Mpp6 regulates the interaction of Nrd1 with nuclear exosome and the C-terminal domain of RNA polymerase II

Kyumin Kim

The yeast saccharomyces cerevisiae Nrd1 interacts with C-terminal domain (CTD) of RNA polymerase II (RNApII) through its CTD-interacting domain (CID) and also associates with the nuclear exosome, thereby acting as both a transcription termination and RNA processing factor. It was recently reported that the Nrd1 CID couples RNApII termination and subsequent RNA processing by recruiting the nuclear exosome to the Nrd1 complex. However, what bridges the Nrd1 CID to the nuclear exosome was not clear. In this study using yeast two hybrid assay, I show two nuclear exosome cofactors, Mpp6 and Trf4 directly and competitively interact with the Nrd1 CID, and regulate the interaction of Nrd1 with RNApII and/or the exosome. Various analyses indicated that Mpp6 promotes the processing of Nrd1-terminated transcripts by Dis3, while Trf4 leads to Rrp6-dependent processing. It implies that Mpp6 and Trf4 may play pivotal roles in choosing a particular RNA processing route within the exosome by guiding the Nrd1-terminated transcripts to their preferred exonucleases.

Key words: Nrd1, Mpp6, RNA polymerase II, Transcription termination, RNA processing

Student number: 2013-22449

TABLE OF CONTENTS

ABSTRACT

TABLE OF CONTENTS

LIST OF FIGURES AND TABLES

INTRODUCTION

RESULTS

1. **Identification of proteins interacting with the Nrd1 CID**
2. **Characterization of Nrd1 CID-Mpp6 interaction**
3. **Mpp6 regulates the interaction between Nrd1 and RNApII**
4. **Mpp6 interacts with Rrp6**
5. **Mpp6 and Trf4 regulate the interaction between Nrd1 and exosome components**
6. **Distinct roles of Mpp6 and Trf4 in coupling Nrd1 to RNA processing by the exosome**

DISCUSSION

MATERIALS AND METHODS

REFERENCES

ABSTRACT IN KOREAN

LIST OF FIGURES AND TABLES

Figure 1. The Nrd1 CID specifically interacts with nuclear exosome co-factors Mpp6 and Trf4.

Figure 2. The binding interfaces of Nrd1 CID for Mpp6 CTD and Trf4 NIM are similar.

Figure 3. Multiple proteins (Mpp6, Trf4 and RNApII CTD) competitively interact with the Nrd1 CID.

Figure 4. Deletion of *MPP6* increases Nrd1 recruitment to 5'-ends of RNApII-transcribed genes.

Figure 5. Nrd1 and RNApII occupancies were monitored by ChIP assay.

Figure 6. Association of various proteins within the exosome/TRAMP complex by Y2H.

Figure 7. Mpp6 and Trf4 regulate the interaction between Nrd1 and exosome components.

Figure 8. Synthetic growth defects of strains.

Figure 9. Distinct roles of Mpp6 and Trf4 in 3'-end processing by the exosome.

Figure 10. Cumulative RNA processing defects for various non-coding RNAs.

Figure 11. Restoration of the Nrd1-Mpp6 interaction rescues cell growth defect.

Figure 12. Model for roles of Mpp6 and Trf4 in Nrd1-dependent termination and RNA processing.

Table 1. Thermodynamic parameters for the complex formation.

Table 2. Yeast strains used in this study

Table 3. ChIP Oligonucleotides used in this study

INTRODUCTION

The Nrd1-Nab3-Sen1 (NNS) complex terminates transcription of small non-coding RNAs by RNApII (Arigo et al, 2006b; Kim et al, 2006; Steinmetz et al, 2001; Thiebaut et al, 2006). Nrd1 and Nab3 are sequence-specific RNA binding proteins and Sen1 (Senataxin in humans) has a RNA/DNA helicase activity that directly dissociates RNApII from the templates (Porrua & Libri, 2013). Nrd1 also recognizes Ser5-phosphorylated (Ser5P) CTD of RNApII using its CID (Vasiljeva et al, 2008). Because the Ser5P CTD is prevalent in the early stage of transcription, the Nrd1 CID-RNApII CTD interaction has been suggested to dictate a regional specificity of NNS-dependent transcription termination (Buratowski, 2009), and a recent CID-swapping experiment satisfyingly confirmed this model (Heo et al, 2013).

The RNAs generated via NNS-dependent termination are trimmed or degraded by the exosome, mediated by Nrd1 complex interactions with this 3'-5' exonuclease (Vasiljeva & Buratowski, 2006). Intriguingly, swapping or deletion of the Nrd1 CID reduced the interaction between Nrd1 and the exosome (Heo et al, 2013), indicating that the Nrd1 CID also plays an important role in coupling termination and RNA processing by recruiting the exosome.

The nuclear exosome consists of the core exosome and a nuclear-specific subunit Rrp6 (PM/Scl100 in humans) that function in RNA 3'-end processing using 3'-5' exoribonuclease activity (Butler, 2002; Houseley & Tollervey, 2009; Liu et al, 2006; Lykke-Andersen et al, 2009). The core exosome is a catalytically inactive barrel-shaped complex composed of nine subunits (Exo-9: RNase PH-like proteins [Rrp41/42/43/45/46, and Mtr3] and S1/KH domain proteins [Rrp4/40, and Csl4]) as well as Dis3 (also known as Rrp44), which is a 3'-5' exo/endonuclease. Being located at the beneath of Exo-9, Dis3 trims or degrades the RNA substrates passed through the central pore of Exo-9 (Schneider

& Tollervey, 2013). In contrast, Rrp6 sits on top of the Exo-9 S1/KH ring above the central channel, and the RNAs traverse the S1/KH ring and enter into the active site of Rrp6 for degradation (Wasmuth et al).

The TRAMP (Trf4/5-Air1/2-Mtr4 polyadenylation) complex is a well-characterized cofactor of the nuclear exosome. It contains a non-canonical poly(A) polymerase, Trf4/5; a putative RNA-binding protein containing zinc knuckle motifs, Air1/2; and the DExH-box RNA helicase, Mtr4. Upon stimulation by the TRAMP complex, the nuclear exosome trims or degrades RNAs (Vanacova et al, 2005; Wyers et al, 2005). Other known cofactors of the nuclear exosome are Rrp47 (C1D in humans) and Mpp6 (Milligan et al, 2008; Mitchell et al, 2003), which preferentially bind to structured and pyrimidine-rich RNAs, respectively (Milligan et al, 2008; Stead et al, 2007). Rrp47 directly interacts with the PMC2NT domain of Rrp6 (Stead et al, 2007) and forms a composite surface for recruiting Mtr4 (Schuch et al, 2014), suggesting that Rrp47 and TRAMP may be functionally linked to the activity of Rrp6. Mpp6 is a nuclear exosome-associated RNA-binding protein involved in 5.8S rRNA maturation in humans (Schilders et al, 2005), and roles in RNA surveillance and degradation of non-coding RNAs have been reported in yeast (Milligan et al, 2008). But the precise role of Mpp6 in exosome function has been unclear.

Despite overlapping enzymatic activities, Rrp6 and Dis3 do not seem to be redundant in RNA processing. For example, Dis3 initially degrades 3'-ends of precursor 5.8S rRNAs and many sn/snoRNAs to make intermediates that are then trimmed to final mature length by Rrp6 (Allmang et al, 2000; van Hoof et al, 2000). Also, Rrp6 carries out some of its critical functions independently of the core exosome (Callahan & Butler, 2008). When tested *in vitro*, selection of RNA degradation by Rrp6 or Dis3 is stochastic (Wasmuth et al, 2014), indicating that there might be a mechanism *in vivo* for choosing a particular RNA degradation route within the exosome. But what regulates the choice and how RNA

substrates are specifically directed to one or the other exonuclease remain largely unknown. In this study, I investigated Nrd1 interactions with the exosome using the yeast two-hybrid (Y2H) assay, and found that the nuclear exosome cofactors Mpp6 and Trf4 directly and mutually exclusively interact with the Nrd1 CID. Deletion of the *MPP6* gene increased Nrd1 recruitment at 5'-ends of genes tested, indicating that Mpp6 may compete for Nrd1-CTD interaction with Ser5P CTD, consequently allowing other factors to bind the RNApII CTD. Mpp6 also promotes the association of Nrd1 with Dis3 via RNA, while Trf4 enhances the Nrd1-Rrp6 interaction. Furthermore, deletion of *MPP6* showed a cumulative RNA processing defect when combined with Rrp6 depletion, while deletion of *TRF4* did so with Dis3 depletion. These results suggest two distinct pathways (Mpp6-Dis3 vs. Trf4-Rrp6) that determine the RNA degradation route within the exosome.

RESULTS

1. Identification of proteins interacting with the Nrd1 CID

Replacing the Nrd1 CID with that of Rtt103 changes not only the CTD-binding specificity of Nrd1, but also the processing of Nrd1-terminated transcripts by exosome because of reduced interaction of Nrd1 with Rrp6 and Trf4 (Heo et al, 2013). Deletion of the Nrd1 CID leads to considerable loss of interaction with Rrp6 and Trf4, suggesting that the Nrd1 CID recruits nuclear exosome and TRAMP complex to the NNS complex. To identify components of nuclear exosome that recognize the Nrd1 CID, I performed the yeast two-hybrid (Y2H) screening using full-length or N-terminal CID (1-154aa) Nrd1 as bait, and found Mpp6 and Trf4 specifically interact with the Nrd1 CID but not the Rtt103 CID (**Figure 1A**).

To validate the Y2H results, TAP-tagged Nrd1 proteins were immunoprecipitated with IgG beads, and associated exosome/TRAMP components (C-terminal 5x myc-tagged) were analyzed by western blotting. Mpp6 and Trf4 co-precipitated with Nrd1 in a CID-dependent, but RNase A-resistant manner (**Figure 1B**), supporting direct interactions of Mpp6 and Trf4 with the Nrd1 CID. Structural evidence for interaction between the Trf4 C-terminus and the Nrd1 CID was also shown recently while this work was in progress (Tudek et al, 2014). Associations of Nrd1 with Rrp6, Sen1, and Rrp4 are also dependent upon the CID and not mediated by RNA (**Figure 1B**), suggesting that the CID may be critical, at least in part, for these proteins to interact with Nrd1. Although the exosome has been shown to associate with Nrd1 (Vasiljeva & Buratowski, 2006), co-IP results revealed that exosome subunits differ in their way to interact with Nrd1: Rrp6 and Rrp4 interact with the CID, Rrp40 and Csl4 interact with Nrd1 independently of the CID and RNA, whereas Dis3,

Rrp41 and Rrp47 indirectly interact with Nrd1 via RNA.

I divided Mpp6 into several parts to narrow down the region interacting with the Nrd1 CID. A segment that contains 140-168 aa (MC-2) interacted with Nrd1 as well as full-length Mpp6 in the Y2H assay (**Figure 1C**). Indeed, this region is critical for interaction, as Nrd1 no longer associates with Mpp6 lacking the MC-2 (**Figure 1D**). This region has multiple glutamic acid residues which may mimic phosphor-serine, and is similar to the Nrd1-interacting motif (NIM) of Trf4 (**Figure 2A**).

A

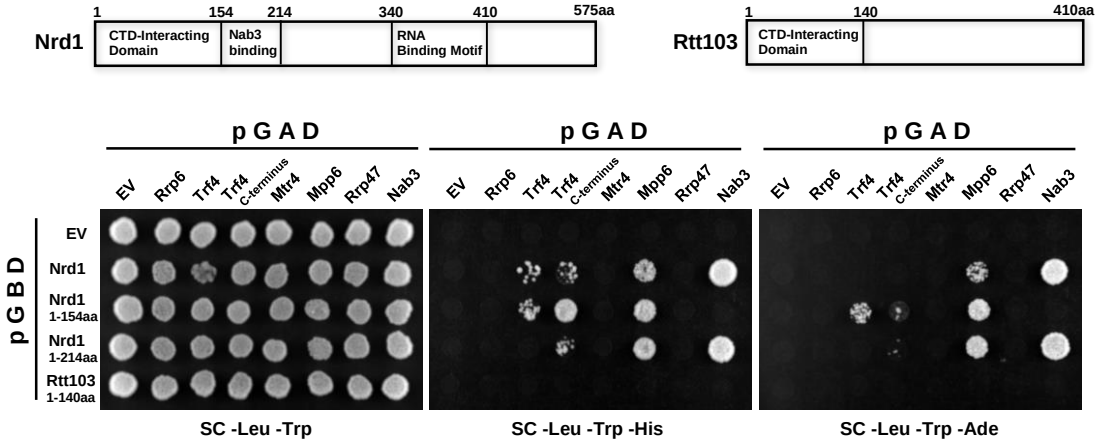
Nrd1
1
154
214
340
410
575aa
CTD-Interacting Domain
Nab3 binding
RNA Binding Motif
Rtt103
1
140
410aa
CTD-Interacting Domain
pGAD
EV
Rrp6
Trf4
Trf4 C-terminus
Mtr4
Mpp6
Rrp47
Nab3
pGBD
EV
Nrd1
Nrd1 1-154aa
Nrd1 1-214aa
Rtt103 1-140aa
SC -Leu -Trp
SC -Leu -Trp -His
SC -Leu -Trp -Ade

B

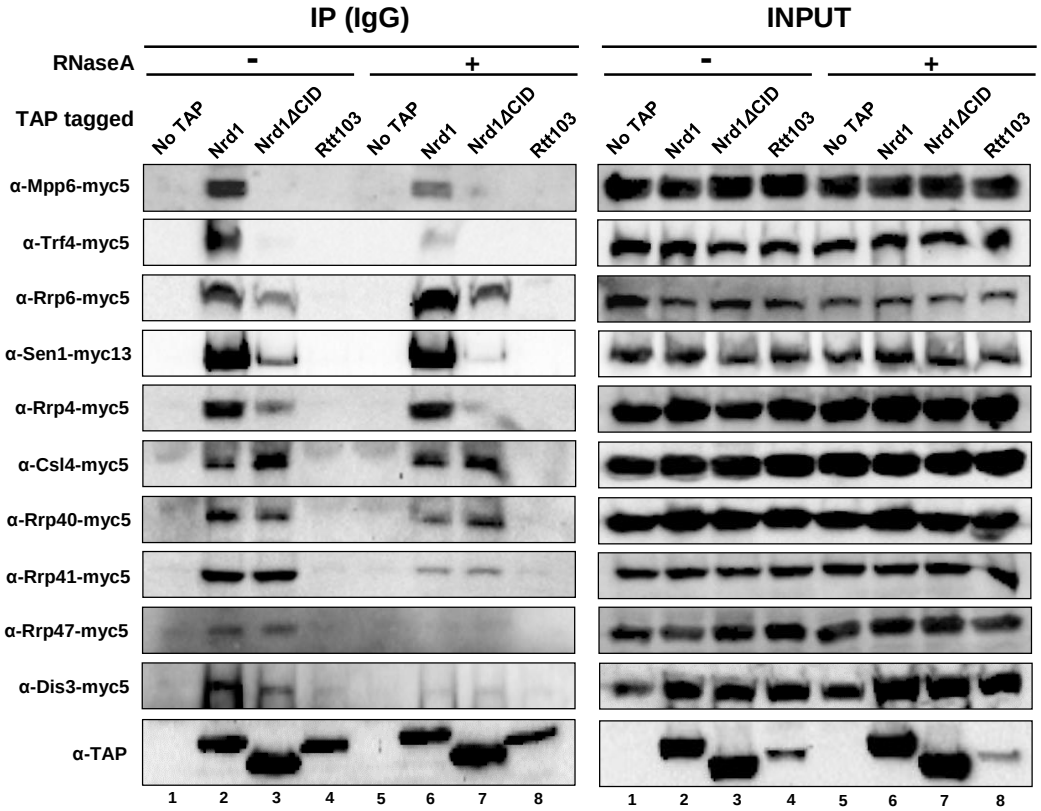
IP (IgG)
INPUT
RNaseA
-
+
TAP tagged
No TAP
Nrd1
Nrd1ΔCID
Rtt103
α-Mpp6-myc5
α-Trf4-myc5
α-Rrp6-myc5
α-Sen1-myc13
α-Rrp4-myc5
α-Csl4-myc5
α-Rrp40-myc5
α-Rrp41-myc5
α-Rrp47-myc5
α-Dis3-myc5
α-TAP
1 2 3 4 5 6 7 8

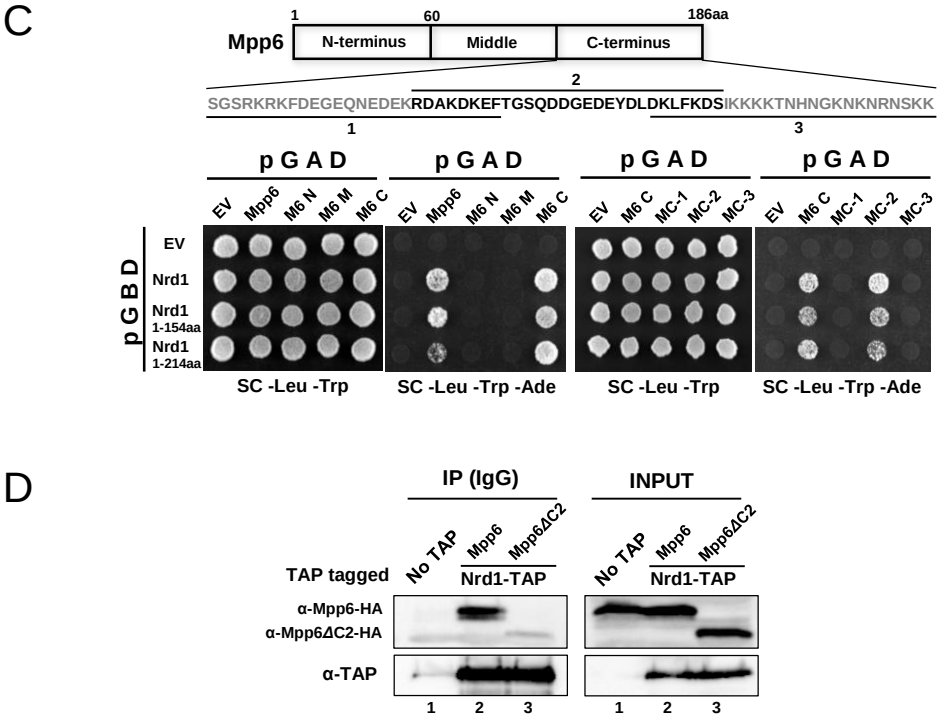

Figure 1. The Nrd1 CID specifically interacts with nuclear exosome co-factors Mpp6 and Trf4.

(**A**) Yeast two-hybrid assay reveals that the CID of Nrd1 interacts with Mpp6 and Trf4. Cells carrying each combination of pGBD (bait) and pGAD (prey) vectors were spotted on indicated plates. Specific protein interactions that allow reporter gene (*HIS3* and *ADE2*) expression lead to cell growth on selective medium. Schematic diagram of Nrd1 and Rtt103 is shown above. Nab3 known to interact with Nrd1 was used as a positive control. EV, empty vector.

(**B**) Co-IP/western blot analysis using C-terminal TAP-tagged Nrd1, Nrd1ΔCID and Rtt103 strains in the absence or presence of RNaseA treatment. After IP with IgG beads, co-IPed proteins were detected using α-myc (9E10) antibody.

(**C**) Mpp6 was divided into several parts, and analyzed by Y2H to identify a region interacting with the Nrd1 CID. Schematic diagram of Mpp6 with corresponding amino acid sequences is shown above.

(**D**) Co-IP/western blot analysis indicates that the Mpp6-C2 region (MC-2) is critical to interact with Nrd1.

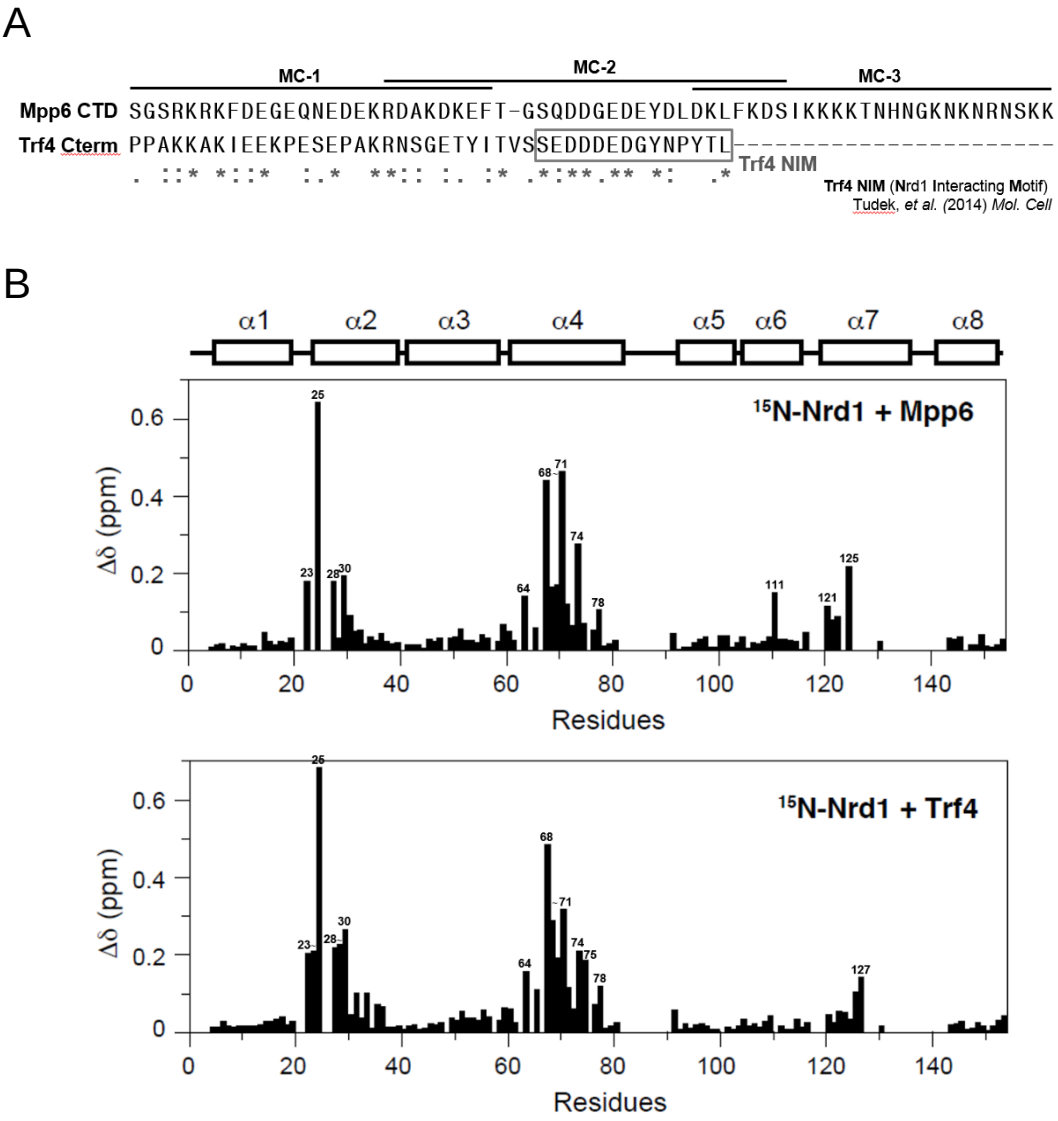

Figure 2. The binding interfaces of Nrd1 CID for Mpp6 CTD and Trf4 NIM are similar.

(**A**) Alignment of Mpp6 CTD and Trf4 C-terminal region using ClustalW2. Mpp6 C1, C2 and C3 regions are denoted by lines; asterisks indicate identical positions, dots and colons denote amino acids with weak and strong similarity, respectively. Trf4 NIM is shown by an open box

(**B**) Quantification of chemical shift perturbations of the Nrd1 CID upon binding to the Mpp6 CTD (upper panel) and the Trf4 NIM (lower panel). Alpha-helix positions of Nrd1 CID are shown above and corresponding residues are marked below

2. Characterization of the Nrd1 CID-Mpp6 interaction

To analyze the binding of Nrd1 CID to Mpp6 and Trf4, backbone chemical shifts of Nrd1 CID in the free state were initially obtained using three-dimensional heteronuclear correlation NMR spectroscopy. Then, chemical shift perturbations (CSP) were measured as ^{15}N-Nrd1 CID was titrated with either the C-terminal domain of Mpp6 (65 aa residues as in **Figure 1C**, referred to as Mpp6 CTD) or the Trf4 NIM using 2D ^{1}H–^{15}N heteronuclear single quantum correlation spectroscopy. The CSP profiles were very similar between two titrations, indicating that the Nrd1 CID largely employed the same binding interfaces for the Mpp6 CTD and the Trf4 NIM (**Figure 2B**). When residues with large CSPs were visualized on the three-dimensional structure of Nrd1, the interfaces were mainly located on α-helices 2, 4, and 7 (**Figure 3A and B**). It is notable that the interaction surfaces also overlap remarkably well with those observed in the complex formed between the Nrd1 CID and Ser5P CTD of RNApII (**Figure 3C**). For example, Ser25 and Arg28, which are critical for the Ser5P CTD binding, showed the largest CSPs. Lys30, Ile68, Ser71, and Arg74 that are in close contact with the Ser5P CTD also exhibited large CSPs for the Mpp6 CTD and the Trf4 NIM. These results strongly suggest that the Nrd1 CID provides a common binding surface to engage with multiple proteins, hence the bindings of Mpp6, Trf4, and Ser5P CTD to the Nrd1 CID should be mutually exclusive with each other.

I measured the binding affinity of Nrd1 CID to the Mpp6 CTD and the Trf4 NIM by isothermal titration calorimetry (ITC). The equilibrium dissociation constant (K_D) between the Nrd1 CID and the Mpp6 CTD was 13.6 μM, and the binding between the Nrd1 CID and the Trf4 NIM showed a K_D of 5.7 μM (**Figure 3D, E and Table 1**). Considering that the affinity of Ser5P CTD (two heptapeptide repeats) for the Nrd1 CID was ~130-fold lower than that of the Trf4 NIM (Tudek et al, 2014), both Mpp6 and Trf4 may be able to displace

the Ser5P CTD of RNApII from the Nrd1 CID. To test this, I performed an *in vitro* binding competition assay using recombinant Nrd1 CID and Mpp6 proteins (**Figure 3F**). The Nrd1 CID was bound to the biotinylated Ser5P CTD peptide (three repeats) immobilized to streptavidin-coated magnetic beads. Adding a molar excess of Mpp6 to this Nrd1-CTD complex led to a significant loss of the Nrd1 CID from the beads, proving that Mpp6 can indeed compete with Ser5P CTD (**Figure 3G**). Similarly, the Nrd1 CID bound to the Trf4 NIM peptide was removed by increasing amounts of Mpp6.

A

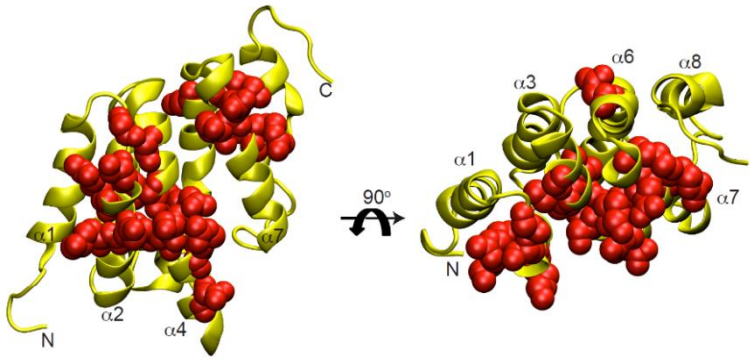
C
α1
α2
α4
α7
N
90°
α3
α6
α8
α1
α7
N

B

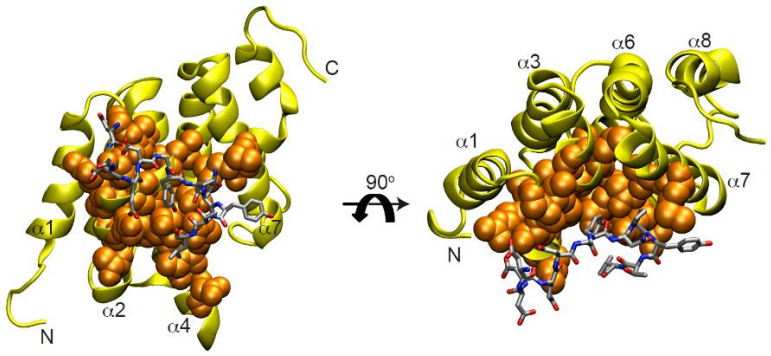
C
α1
α2
α4
α7
N
90°
α3
α6
α8
α1
α7
N

C

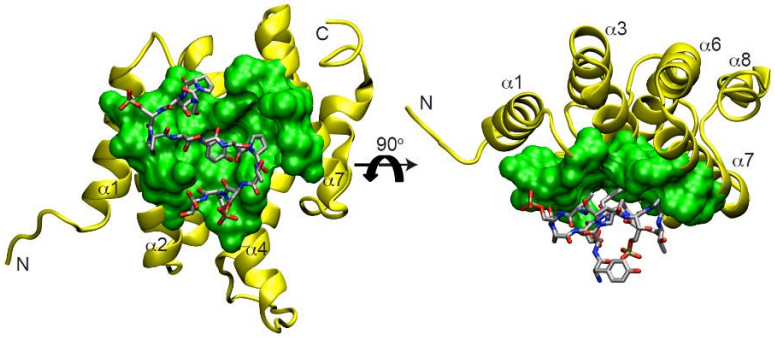
C
α1
α2
α4
α7
N
90°
N
α3
α6
α8
α1
α7

D

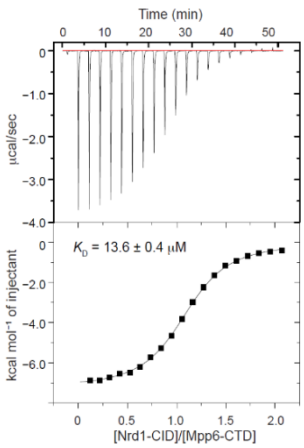
Time (min)
0
10
20
30
40
50
μcal/sec
0
-1.0
-2.0
-3.0
-4.0
K_D = 13.6 ± 0.4 μM
kcal mol⁻¹ of injectant
0
-2.0
-4.0
-6.0
0
0.5
1.0
1.5
2.0
[Nrd1-CID]/[Mpp6-CTD]

E

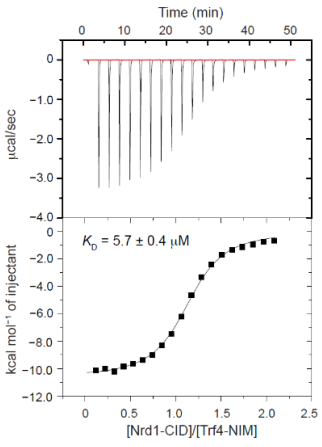
Time (min)
0
10
20
30
40
50
μcal/sec
0
-1.0
-2.0
-3.0
-4.0
K_D = 5.7 ± 0.4 μM
kcal mol⁻¹ of injectant
0
-2.0
-4.0
-6.0
-8.0
-10.0
-12.0
0
0.5
1.0
1.5
2.0
2.5
[Nrd1-CID]/[Trf4-NIM]

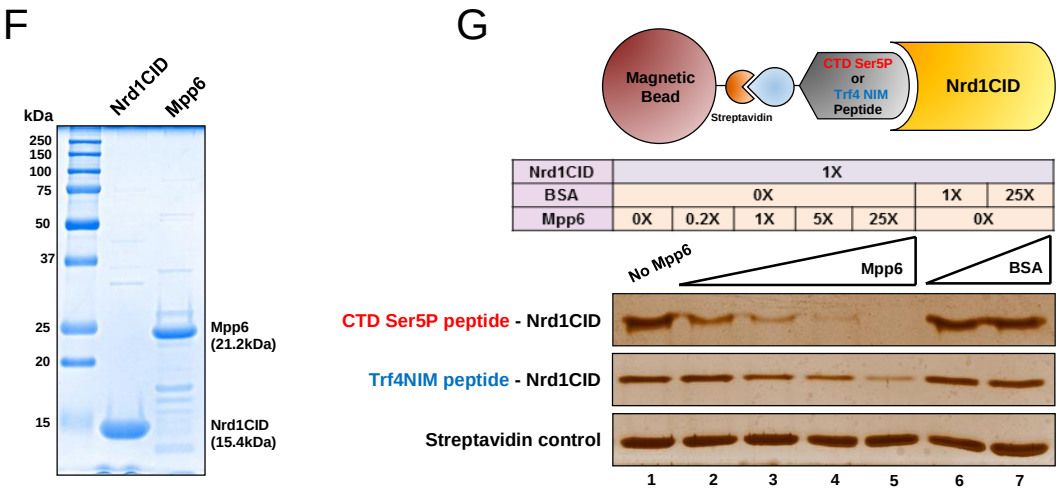

Figure 3. Multiple proteins (Mpp6, Trf4 and RNApII CTD) competitively interact with the Nrd1 CID.

(A, B) The Nrd1 CID is shown in a ribbon diagram representation, and the chemical shift perturbation is shown as a space-filling model for Mpp6 CTD (A), and Trf4 NIM peptide (B) (PDB code 1LO6).

(C) The interaction surface for Ser5P CTD is drawn as a surface diagram (PDB code 2MOW). The Trf4 NIM and Ser5P CTD peptides bound to the Nrd1 CID (26) are shown as a stick representation in (B) and (C)

(D, E) Raw ITC data (top panels) and integrated heats of injection (bottom panels) for Nrd1 CID/Mpp6 CTD (D) and Nrd1 CID/Trf4 NIM (E) titration at 25°C. Squares in the bottom panels are experimental data; red line represents the least-squares best fit curves derived from a simple one-site binding model.

(F) Recombinant Nrd1 CID and Mpp6 proteins were purified and analyzed by SDS-PAGE and coomassie blue staining.

(G) Binding competition assay. Biotinylated-peptide (Ser5P CTD [three repeats] or Trf4 NIM) was immobilized to streptavidin-coated magnetic beads, and bound to recombinant Nrd1 CID protein (Schematic representation is shown above). Increasing amounts of recombinant Mpp6 protein were added to the mixture, and the remaining amounts of Nrd1 CID bound to the beads were monitored by SDS-PAGE and silver staining

Description	K_D **(**μM**)**	ΔG **(kcal/mol)**	ΔH **(kcal/mol)**	$-T\Delta S$ **(kcal/mol)**
Nrd1 CID + Trf4 NIM	5.7 ± 0.4	–7.2 ± 0.5	–10.6 ± 0.1	3.4 ± 0.5
Nrd1 CID + Mpp6 CTD	13.6 ± 0.4	–6.6 ± 0.2	–7.3 ± 0.0	0.7 ± 0.2

Table 1. Thermodynamic parameters for the complex formation between Nrd1 CID and Trf4 NIM, and between Nrd1 CID and Mpp6 CTD obtained by isothermal titration calorimetry at 25°C.

3. Mpp6 regulates the interaction between Nrd1 and RNApII

Since the original role of CID is to recruit Nrd1 to the early elongating RNApII via Ser5P CTD (Vasiljeva et al, 2008), I investigated whether Mpp6 and Trf4 affect the interaction of Nrd1 with RNApII during transcription by chromatin immunoprecipitation assay. Indeed, the recruitment of TAP-tagged Nrd1 at 5'-ends of genes was significantly increased in *mpp6Δ* mutant (**Fig 4A-C and Figure 5**). The absence of Mpp6 does not change the level of Ser5P CTD, but allows increased interaction of Nrd1 with Ser5P CTD of RNApII (**Figure 4D and E**). Thus, Mpp6 may fine-tune the interaction between Nrd1 and RNApII at 5'-ends of genes by competing with Ser5P CTD. Notably, deletion of *TRF4* barely increases the recruitment of Nrd1 at 5'-ends (**Figure 4A-C**), which suggests that Mpp6 and Trf4 are temporally distinct in regulating the association of Nrd1 with other proteins via the CID.

To test whether the increased recruitment of Nrd1 to elongating RNApII leads to termination defects, I analyzed RNApII occupancy on the *NRD1* gene, which is autoregulated via premature termination by NNS (Arigo et al, 2006a). In the *mpp6Δ* mutant, premature termination at the 5'-end of *NRD1* was considerably diminished, and the steady-state *NRD1* mRNA level was increased accordingly (**Figure 4F and G**), confirming a role of Mpp6 in Nrd1-dependent termination. As previously reported (Arigo et al, 2006a), a *trf4Δ* mutant also showed a termination defect, even though it did not alter the Nrd1 recruitment at 5'-ends of genes tested (**Figure 4F**). This suggests that Trf4 affects Nrd1-dependent termination differently from Mpp6.

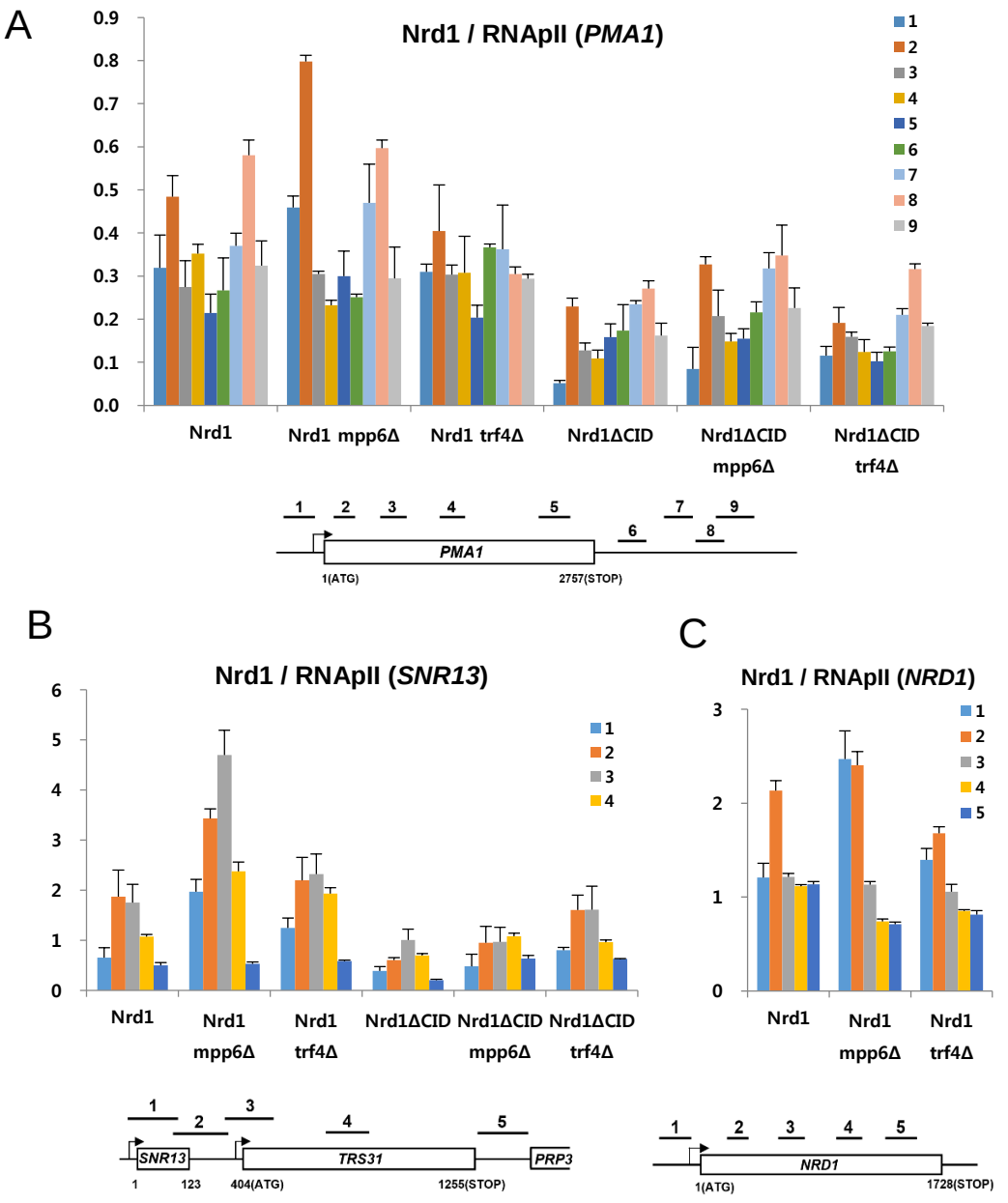
A
Nrd1 / RNApII (PMA1)
0.9
0.8
0.7
0.6
0.5
0.4
0.3
0.2
0.1
0.0
1
2
3
4
5
6
7
8
9
Nrd1
Nrd1 mpp6Δ
Nrd1 trf4Δ
Nrd1ΔCID
Nrd1ΔCID mpp6Δ
Nrd1ΔCID trf4Δ
1 2 3 4 5 6 7 8 9
PMA1
1(ATG)
2757(STOP)
B
Nrd1 / RNApII (SNR13)
6
5
4
3
2
1
0
1
2
3
4
Nrd1
Nrd1 mpp6Δ
Nrd1 trf4Δ
Nrd1ΔCID
Nrd1ΔCID mpp6Δ
Nrd1ΔCID trf4Δ
1 2 3 4 5
SNR13
TRS31
PRP3
1
123
404(ATG)
1255(STOP)
C
Nrd1 / RNApII (NRD1)
3
2
1
0
1
2
3
4
5
Nrd1
Nrd1 mpp6Δ
Nrd1 trf4Δ
1 2 3 4 5
NRD1
1(ATG)
1728(STOP)
D
CTD Ser5P level (PMA1)
700
600
500
400
300
200
100
0
1
2
3
4
5
6
7
8
9
Nrd1
Nrd1 mpp6Δ
E
IP (IgG)
INPUT
No TAP
Nrd1-TAP
Nrd1-TAP mpp6Δ
No TAP
Nrd1-TAP
Nrd1-TAP mpp6Δ
α-CTDS5P
α-TAP
1 2 3 1 2 3

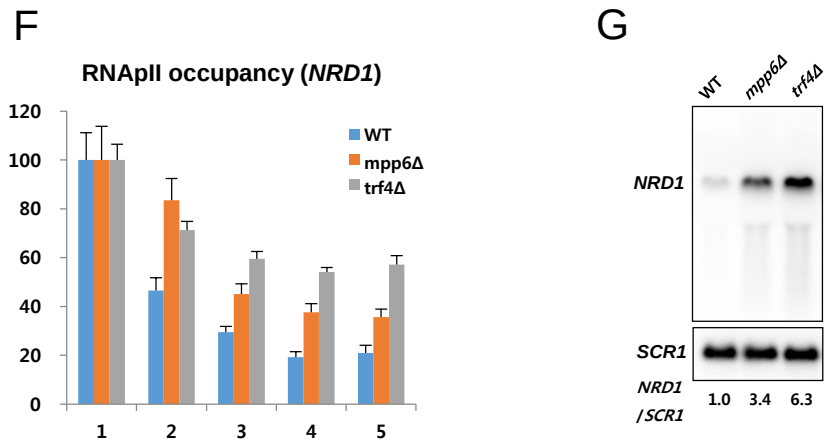

Figure 4. Deletion of *MPP6* increases the Nrd1 recruitment to 5'-ends of RNApII-transcribed genes.

(**A-C**) Recruitment of C-terminal TAP-tagged Nrd1 was monitored by chromatin immunoprecipitation (ChIP) assay in indicated strains. The same chromatin preparations were also used to analyze RNApII occupancy using α-Rpb3 antibody (See **Figure 5**). Finally, the level of Nrd1 occupancy normalized to RNApII occupancy is shown here. *PMA1* gene (A). *SNR13* gene (B). *NRD1* gene (C). Schematic representation of genes analyzed is shown below; arrows indicate promoters; numbered bars denote positions of the PCR products used in ChIP analysis.

(**D**) The level of Ser5P CTD was measured by ChIP using 3E8 antibody on the *PMA1 gene* in wild-type and *mpp6Δ* cells. Positions of PCR primers as shown in (A).

(**E**) Co-IP/western blot analysis using C-terminal TAP-tagged Nrd1 in wild-type and *mpp6Δ* backgrounds. The association of Nrd1 with Ser5P CTD increases upon deletion of *MPP6*.

(**F**) RNApII occupancy was monitored by ChIP in wild-type, *mpp6Δ,* and *trf4Δ* cells. Signals at the promoter were set to 100 and those from other positions were calculated in relative amounts.

(**G**) Steady-state *NRD1* mRNA level was analyzed by Northern blot in *mpp6Δ* and *trf4Δ* mutants. Probe location is shown in (C). *SCR1* serves as a loading control; the relative ratio of *NRD1* to *SCR1* is shown below. *Error bars* represent S.E. for at least three independent experiments.

A

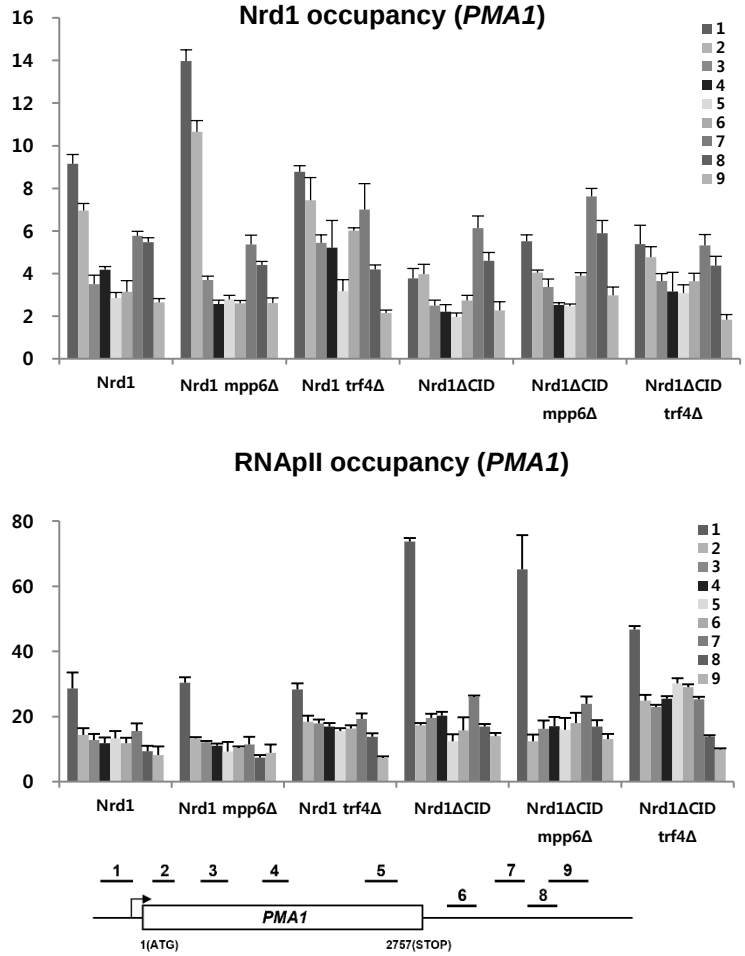
Nrd1 occupancy (PMA1)
16
14
12
10
8
6
4
2
0
1
2
3
4
5
6
7
8
9
Nrd1
Nrd1 mpp6Δ
Nrd1 trf4Δ
Nrd1ΔCID
Nrd1ΔCID mpp6Δ
Nrd1ΔCID trf4Δ
RNApII occupancy (PMA1)
80
60
40
20
0
1
2
3
4
5
6
7
8
9
Nrd1
Nrd1 mpp6Δ
Nrd1 trf4Δ
Nrd1ΔCID
Nrd1ΔCID mpp6Δ
Nrd1ΔCID trf4Δ
1
2
3
4
5
6
7
8
9
PMA1
1(ATG)
2757(STOP)

B

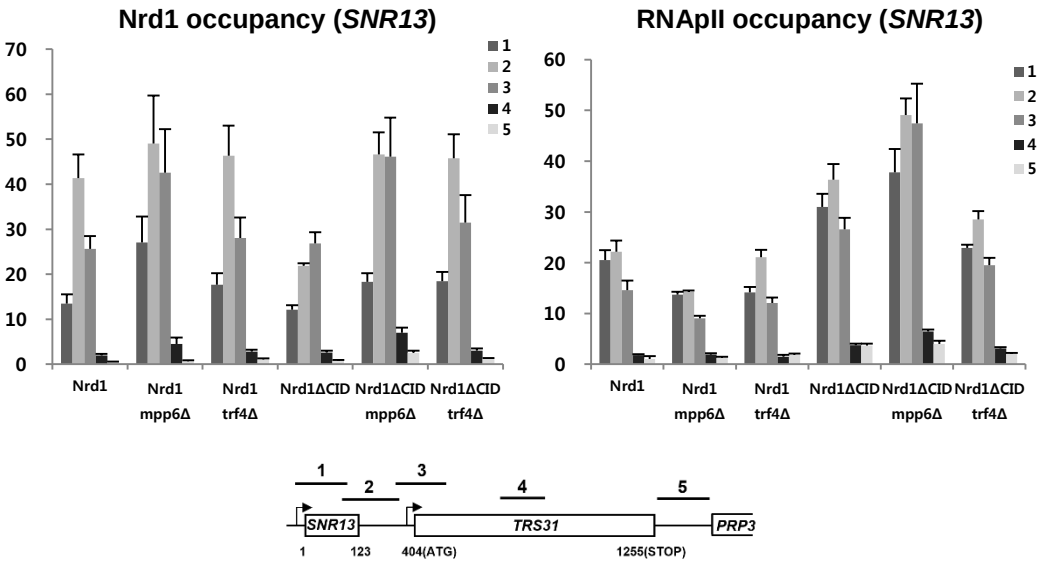
Nrd1 occupancy (SNR13)
70
60
50
40
30
20
10
0
1
2
3
4
5
Nrd1
Nrd1 mpp6Δ
Nrd1 trf4Δ
Nrd1ΔCID
Nrd1ΔCID mpp6Δ
Nrd1ΔCID trf4Δ
RNApII occupancy (SNR13)
60
50
40
30
20
10
0
1
2
3
4
5
Nrd1
Nrd1 mpp6Δ
Nrd1 trf4Δ
Nrd1ΔCID
Nrd1ΔCID mpp6Δ
Nrd1ΔCID trf4Δ
1
2
3
4
5
SNR13
TRS31
PRP3
1
123
404(ATG)
1255(STOP)

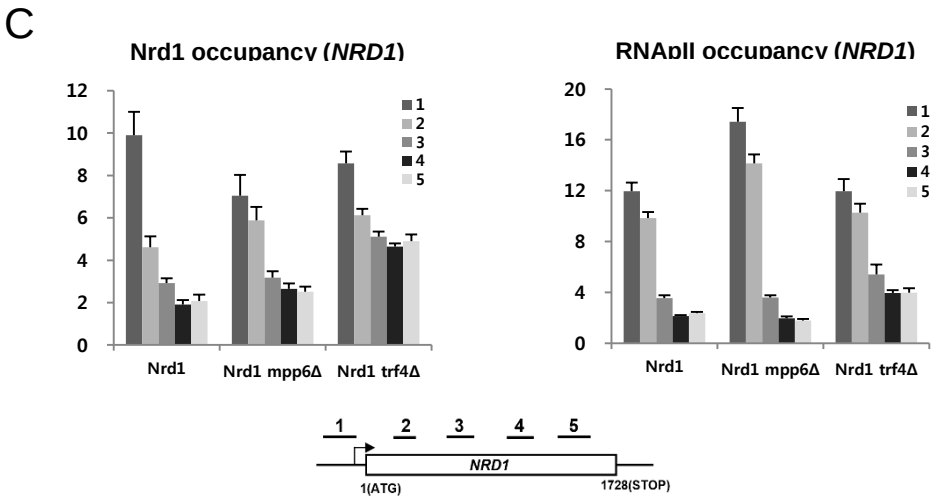

Figure 5. Nrd1 and RNApII occupancies were monitored by ChIP assay.

(**A-C**) Schematic representation of genes analyzed is shown below; arrows indicate promoters; numbered bars denote positions of the PCR products used in PCR analysis. *Error bars* represent S.E. for at least three independent experiments. *PMA1* gene (A). *SNR13* gene (B). *NRD1* gene (C).

4. Mpp6 interacts with Rrp6

Human Mpp6 interacts directly with PM-Scl100 (human Rrp6) and hMtr4 by Y2H and co-IP experiments using recombinant and *in vitro* translated proteins (Lehner & Sanderson, 2004; Schilders et al, 2007). I consistently found that yeast Mpp6 also interacts with Rrp6 and Mtr4 by Y2H assay, although the interaction between Mpp6 and Mtr4 was much weaker than the Mpp6-Rrp6 interaction as judged by the cell growth on selective medium (**Figure 6A**). While components of TRAMP complex (Trf4 and Mtr4) interact with each other, I did not observe the interactions of Trf4 and Mtr4 with Rrp6. Rrp6 also interacts with several core exosome subunits (Csl4, Rrp41, Rrp43), but none of the core exosome subunits tested interacts with TRAMP (Trf4, Mtr4), Mpp6, or Rrp47 in Y2H assay (**Figure 6B**), implying that major roles of these factors could be to modulate the activity of Rrp6 and/or its RNA substrate specificity. Recently, a size-exclusion chromatography study using purified proteins showed that Mpp6 binds to the exosome core (Exo-9) (Schuch et al, 2014). Mpp6 may interact with other core exosome subunits (Rrp42, Mtr3, Rrp46, and Rrp45) I have not tested in Y2H or recognize the interface between subunits. In either case, this suggests that Mpp6 has another role in RNA processing independent of Rrp6.

Mpp6 and Rrp47 do not interact with each other (**Figure 6A**), but bind to distinct domains within Rrp6: Mpp6 binds to the central EXO domain, while Rrp47 binds to the N-terminal PMC2NT domain (**Figure 6C**). This suggests that a stable Mpp6-Rrp6-Rrp47 complex can assemble as previously shown *in vitro* using human proteins (Schilders et al, 2007). Importantly, the region (MC-2) within Mpp6 that binds to the Nrd1 CID turns out to mediate the interaction with Rrp6 as well (**Figure 6D**). Therefore, Mpp6 may not be able to bind to Nrd1 and Rrp6 simultaneously.

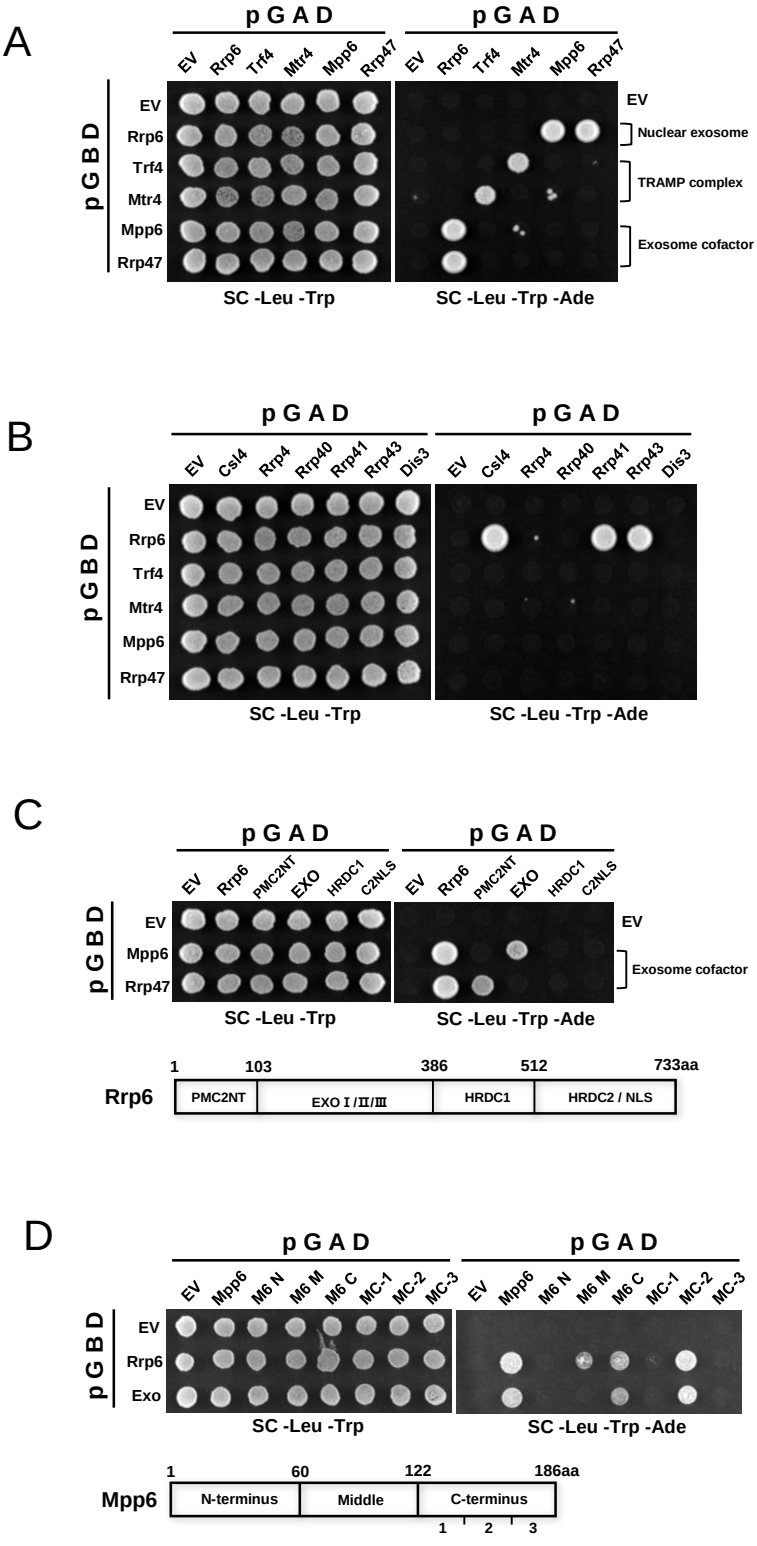
A
p G A D
EV
Rrp6
Trf4
Mtr4
Mpp6
Rrp47
p G B D
Nuclear exosome
TRAMP complex
Exosome cofactor
SC -Leu -Trp
SC -Leu -Trp -Ade
B
Csl4
Rrp4
Rrp40
Rrp41
Rrp43
Dis3
C
PMC2NT
EXO
HRDC1
C2NLS
Rrp6
1
103
386
512
733aa
PMC2NT
EXO Ⅰ/Ⅱ/Ⅲ
HRDC1
HRDC2 / NLS
D
Mpp6
M6 N
M6 M
M6 C
MC-1
MC-2
MC-3
Exo
60
122
186aa
N-terminus
Middle
C-terminus

Figure 6. Association of various proteins within the exosome/TRAMP complex by Y2H assay.

(**A-D**) Cell suspensions were spotted on plates lacking adenine (right panel) to monitor *ADE2* expression indicating two-hybrid interaction. (A) Mpp6 interacts with Rrp6 and Mtr4 (weak), and Rrp6 does with Mpp6 and Rrp47. (B**)** Rrp6 interacts with Csl4, Rrp41, and Rrp43 of the core exosome. (C) Mpp6 and Rrp47 interact with distinct domains within Rrp6. Schematic diagram of Rrp6 is shown below. (D) The C-terminal portion (MC-2) of Mpp6 that interacts with the Nrd1 CID is also required for binding the EXO domain of Rrp6. Schematic diagram of Mpp6 is shown below as in **Figure 1C**.

5. Mpp6 and Trf4 regulate the interaction between Nrd1 and exosome components

To investigate how Mpp6 and Trf4 affect the association of Nrd1 with nuclear exosome, I performed co-IP experiments. Deletion of *MPP6* increases the Nrd1-Rrp6 interaction, but decreases the Nrd1-Dis3 interaction (**Figure 7A**). However, deletion of *TRF4* leads to opposite outcomes: decrease in the Nrd1-Rrp6 interaction, but increase in the Nrd1-Dis3 interaction (**Figure 7B**). Since the level of TAP-tagged Nrd1 increases in *mpp6Δ* and *trf4Δ* mutants presumably due to the increase of *NRD1* mRNA level (**Figure 4G**), changes in the interactions of Nrd1 with various factors were normalized against the increase and shown in relative numbers (**Figure 7C and D**). These results indicate that Mpp6 promotes Nrd1 to associate with Dis3 via RNA, while Trf4 facilitates Nrd1 to associate with Rrp6 via protein-protein interaction. The association of Nrd1 with Trf4 and Sen1 increases in the *mpp6Δ* mutant and so does the association of Nrd1 with Mpp6 and Sen1 in the *trf4Δ* mutant, likely because these proteins (Mpp6, Trf4, and Sen1) are competing with each other for the Nrd1 CID. The probable interaction between Sen1 and the Nrd1 CID may assist dissociation of Nrd1 from Ser5P CTD, which in turn facilitate association of Sen1 with Ser2P CTD (Chinchilla et al, 2012) during the transition from initiation to elongation phase of transcription.

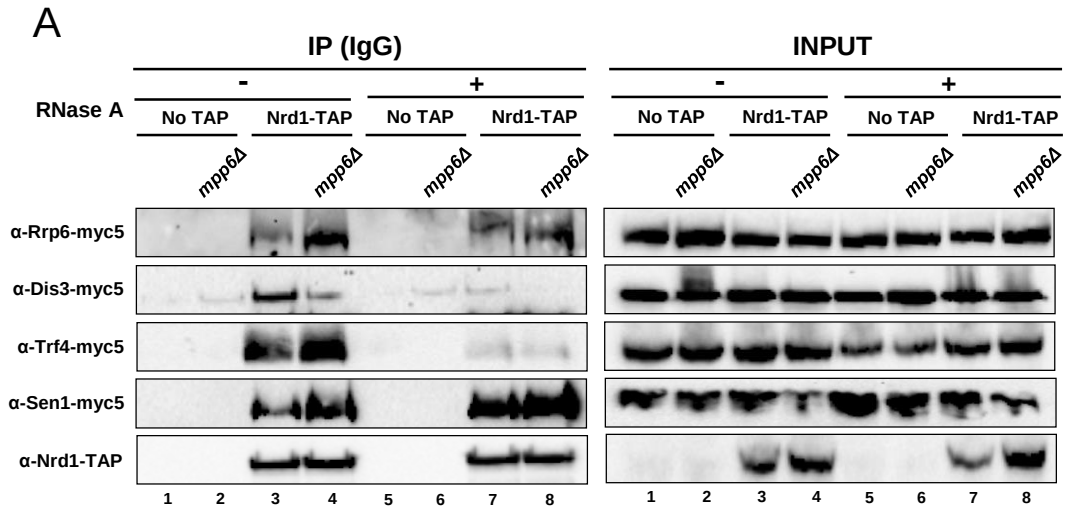

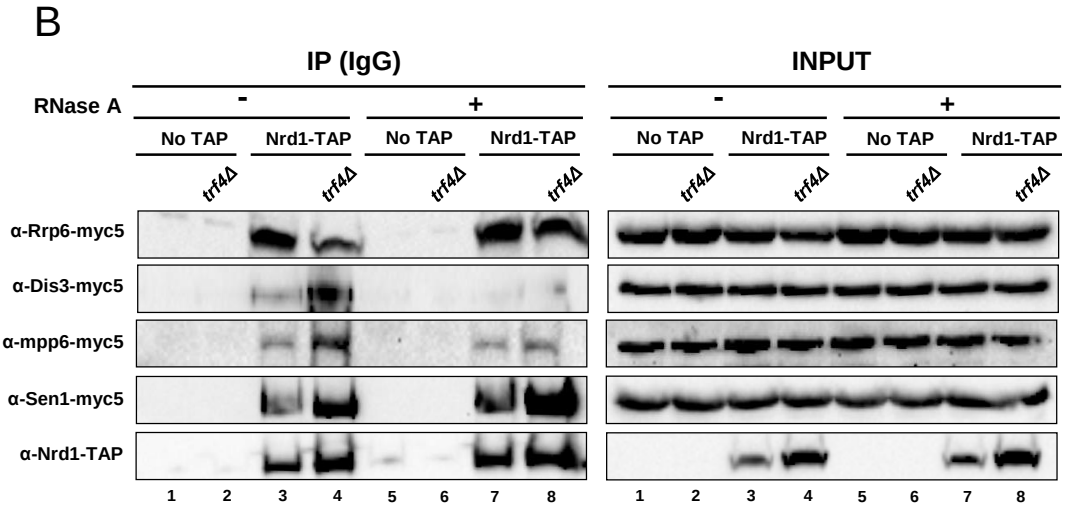

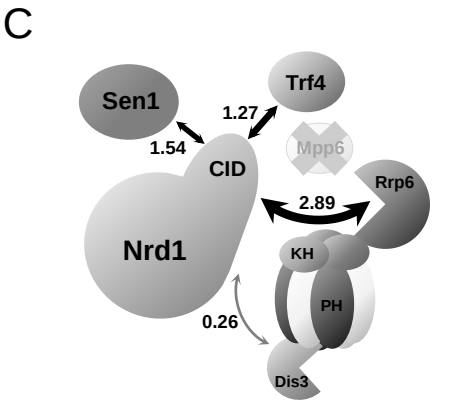

$$\text{Relative fold changes in interaction} = \frac{\frac{\text{IP-myc } mpp6\Delta}{\text{IP-Nrd1 } mpp6\Delta}\ \text{(Lane 4)}}{\frac{\text{IP-myc } WT}{\text{IP-Nrd1 } WT}\ \text{(Lane 3)}}$$

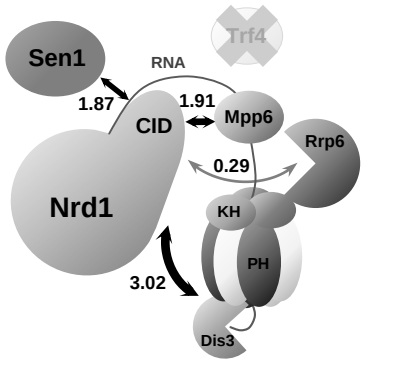

$$\text{Relative fold changes in interaction} = \frac{\frac{\text{IP-myc } trf4\Delta}{\text{IP-Nrd1 } trf4\Delta}\ \text{(Lane 4)}}{\frac{\text{IP-myc } WT}{\text{IP-Nrd1 } WT}\ \text{(Lane 3)}}$$

Figure 7. Mpp6 and Trf4 regulate the interaction between Nrd1 and exosome components.

(**A, B**) Co-IP/western blot analyses were performed using C-terminal TAP-tagged Nrd1 in the absence or presence of RNaseA treatment. After IP with IgG beads, co-IPed proteins from *mpp6Δ* (A) or *trf4Δ* (B) mutant were detected and compared to wild-type control by using α-myc (9E10) antibody.

(**C, D**) Results from (A) and (B) are illustrated in *mpp6Δ* (C) and *trf4Δ* (D) mutant, respectively. Arrow thickness denotes the extent of interaction between proteins. Numbers represent relative fold changes in the interactions of Nrd1 with exosome components upon deletion of *MPP6* or *TRF4*. These were also normalized against the increased level of Nrd1-TAP in deletion mutants.

6. Distinct roles of Mpp6 and Trf4 in coupling Nrd1 to RNA processing by the exosome.

I monitored how the altered association of Nrd1 with two exonucleases subsequently affects the RNA processing of Nrd1-terminated transcripts by Northern blotting. Since deleting both *MPP6* and *RRP6* causes cell lethality (Milligan et al, 2008), I depleted Rrp6 using a repressible Gal promoter (*pGal-RRP6*) in *mpp6Δ* mutant. Deletion of *MPP6* alone had no obvious RNA processing defect, while depletion of Rrp6 led to small amounts of unprocessed snoRNA transcripts (pre-snoRNA, marked in black arrowhead). When depletions of these two factors were combined, the cells failed to grow on glucose (**Figure 8A**) and pre-snoRNAs were massively accumulated for both *SNR13* and *SNR33* (**Figure 9A**, compare lanes 6 and 8). Based upon these results, I propose that deletion of *MPP6* renders the RNA processing of Nrd1-terminated transcripts more dependent upon Rrp6, as Mpp6 is no longer present to guide the transcripts toward Dis3. In Nrd1ΔCID background, however, the pre-snoRNA accumulation in *mpp6Δ pGal-RRP6* mutant was reduced (**Figure 9A**, compare lanes 8 and 16), presumably because Trf4 that facilitates the Nrd1-Rrp6 association cannot take part in the process either, due to lack of the CID, thus limiting the contribution of Rrp6 in trimming the Nrd1-terminated transcripts.

In contrast, when *mpp6Δ* was combined with Dis3 depletion using *pGal-DIS3*, accumulation of pre-snoRNAs was not considerably increased relative to Dis3 depletion alone (**Figure 9B**, lanes 6 and 8). The lack of additive effect between Mpp6 and Dis3 predicts that these two proteins act in the same processing pathway. Besides, deletion of the Nrd1 CID did not significantly change the level of premature transcripts (**Figure 9B**, lanes 8 and 16). It is likely because deletion of the CID would have the same effect as deletion of *MPP6* on the association of Nrd1 with Dis3 (**Figure 1B** and **Figure 7A**).

Double deletion of *MPP6* and *TRF4* resulted in a cell growth defect (**Figure 8B**) and

synergistic accumulation of pre-snoRNAs (**Figure 9C**, lanes 2-4), indicating that Mpp6 and Trf4 are in the separate pathways. TRAMP is known to enhance RNA degradation by Rrp6 independently of the core exosome (Callahan & Butler, 2008), and Trf4 (a component of TRAMP) facilitates the association between Nrd1 and Rrp6 (**Figure 7B**). These findings illustrate that Trf4 and Rrp6 comprise a RNA processing pathway distinct from the one with Mpp6 and Dis3 (**Figure 9D**). To validate this model, I simultaneously disrupted two proteins either in the same pathway or in the separate pathways, and monitored probable cumulative RNA processing defect. Indeed, *mpp6Δ* accumulated a much higher level of pre-snoRNAs when combined with *pGal-RRP6* (separate pathway) than *pGal-DIS3* (same pathway) (**Figure 9E, F and Figure 10**, compare lanes 12 and 14). Similarly, *trf4Δ* produced greater amounts of premature transcripts with *pGal-DIS3* (separate pathway) than *pGal-RRP6* (same pathway) (**9E, F and Figure 10**, compare lanes 16 and 18). These results support the existence of two distinct pathways within the exosome that process the Nrd1-terminated transcripts. Consistent with this, a synthetic growth defect seen in *mpp6Δ pGal-RRP6* and *mpp6Δ trf4Δ* mutants was rescued by wild-type Mpp6 but not by Mpp6ΔC2 lacking the Nrd1-interacting domain (**Figure 11**), elucidating that maintaining at least one alternative RNA processing route is essential for cell viability.

To further assess the Mpp6-Dis3 and Trf4-Rrp6 linkages, I examined the exonuclease activity of Dis3 and Rrp6 isolated from *mpp6Δ* or *trf4Δ* mutant using a 5'-labeled synthetic RNA substrate derived from the *SNR13* 3'-end region. The 3'-5' exonuclease activity of Dis3 was severely reduced by deletion of *MPP6*, but deletion of *TRF4* showed only a marginal effect (**Figure 9G**, left). On the contrary, the activity of Rrp6 was more strongly affected by deletion of *TRF4* rather than *MPP6* (**Figure 9G**, right). These results confirm that Mpp6 promotes RNA degradation by Dis3, while Trf4 does so by Rrp6. I therefore conclude that Mpp6 and Trf4 are actively involved in selection of a RNA processing route

by directing transcripts to their associated exonuclease (**Figure 12**).

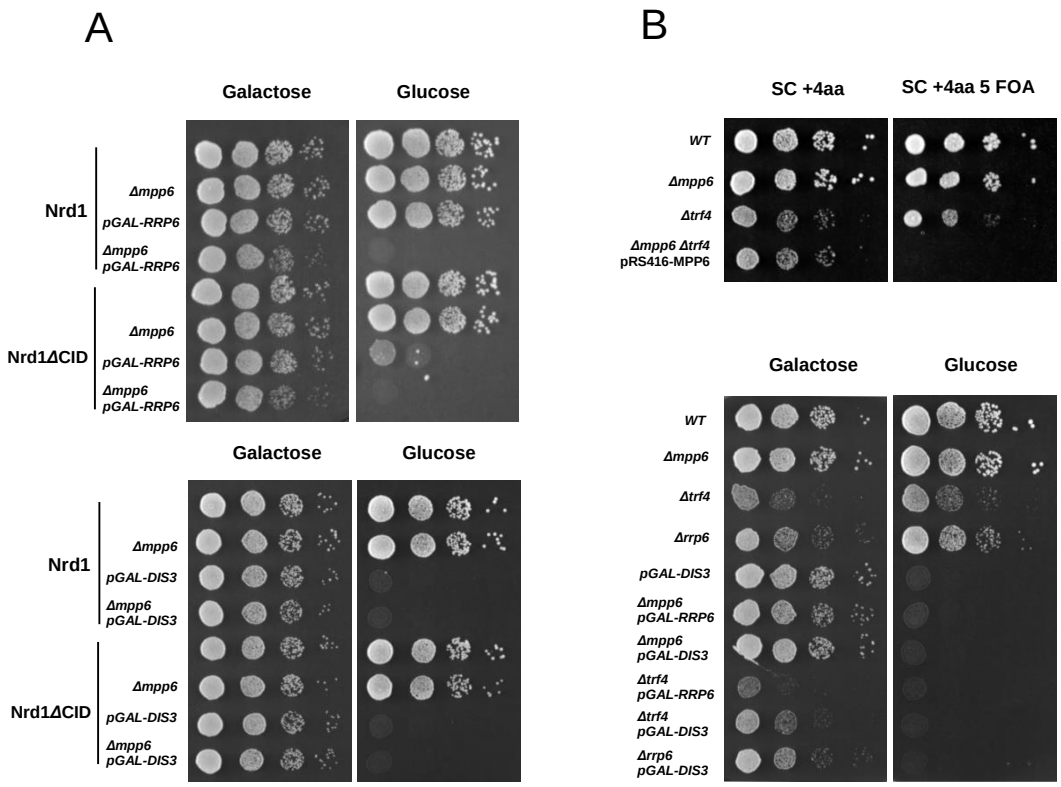

Figure 8. Synthetic growth defects of strains.

(**A, B**) Ten-fold serial dilutions of cell cultures were spotted onto indicated medium plates and incubated at 30℃ for 2 days. *mpp6Δ pGAL-RRP6* and *mpp6Δ pGAL-DIS3* strains (A). *mpp6Δ trf4Δ* strains and various combinations of deletion and depletion strains (B).

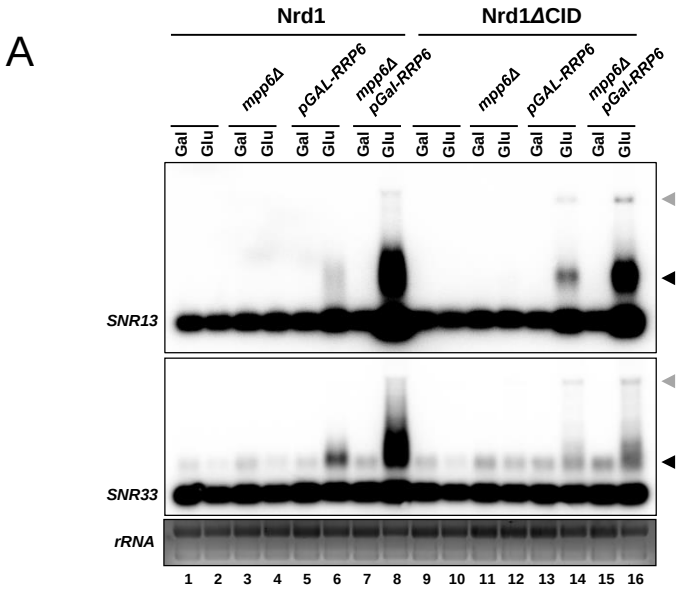
A
Nrd1
Nrd1ΔCID
mpp6Δ
pGAL-RRP6
mpp6Δ pGal-RRP6
Gal
Glu
SNR13
SNR33
rRNA
1 2 3 4 5 6 7 8 9 10 11 12 13 14 15 16

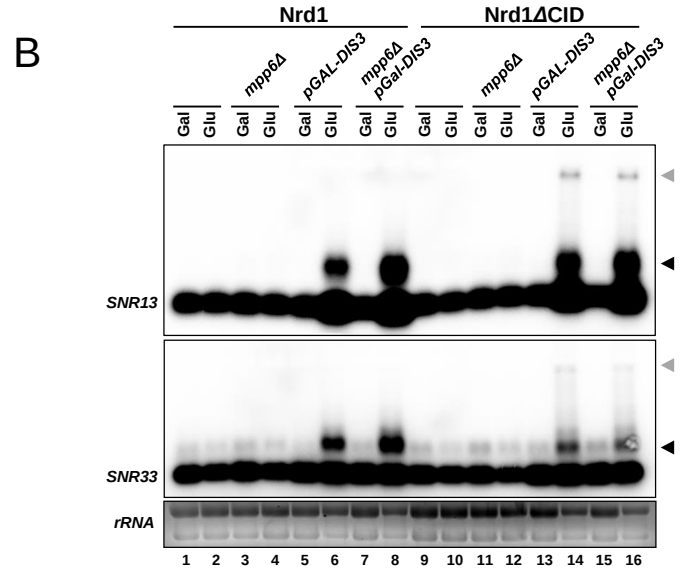
B
Nrd1
Nrd1ΔCID
mpp6Δ
pGAL-DIS3
mpp6Δ pGal-DIS3
Gal
Glu
SNR13
SNR33
rRNA
1 2 3 4 5 6 7 8 9 10 11 12 13 14 15 16

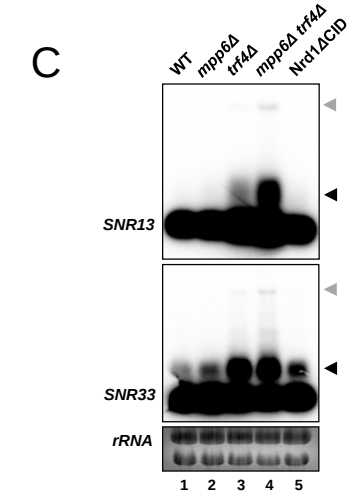
C
WT
mpp6Δ
trf4Δ
mpp6Δ trf4Δ
Nrd1ΔCID
SNR13
SNR33
rRNA
1 2 3 4 5

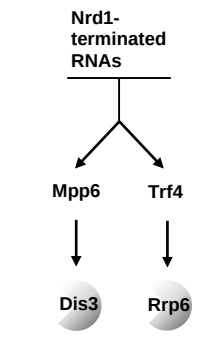
D
Nrd1-terminated RNAs
Mpp6
Trf4
Dis3
Rrp6

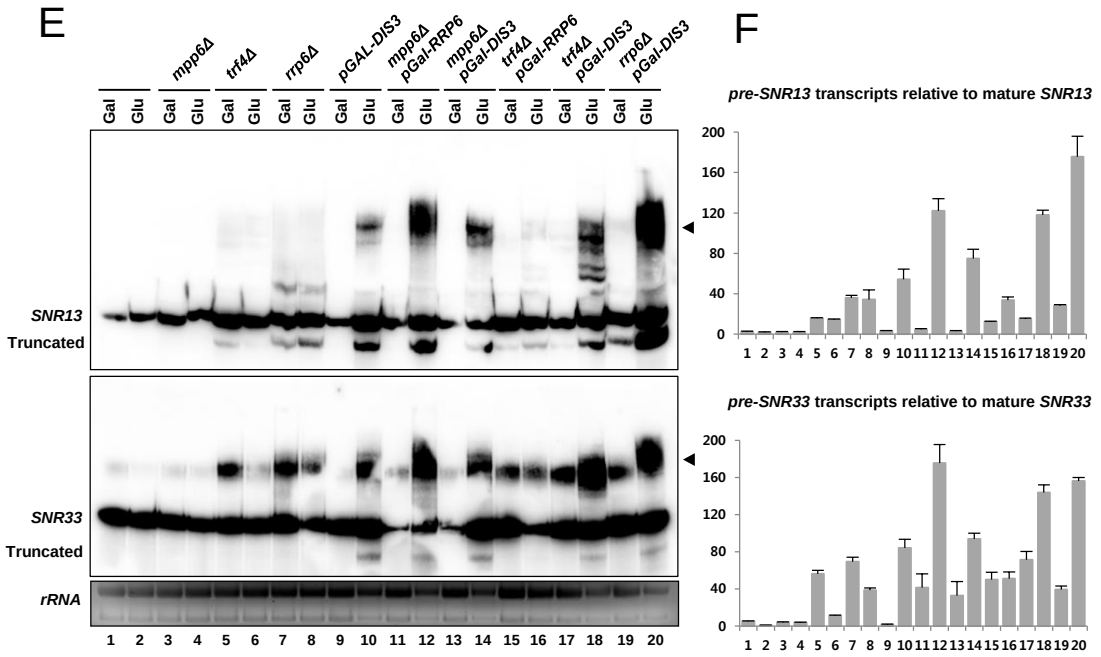
E
mpp6Δ
trf4Δ
rrp6Δ
pGAL-DIS3
mpp6Δ pGal-RRP6
mpp6Δ pGal-DIS3
trf4Δ pGal-RRP6
trf4Δ pGal-DIS3
rrp6Δ pGal-DIS3
Gal Glu
SNR13
Truncated
SNR33
Truncated
rRNA
1 2 3 4 5 6 7 8 9 10 11 12 13 14 15 16 17 18 19 20
F
pre-SNR13 transcripts relative to mature SNR13
pre-SNR33 transcripts relative to mature SNR33
0 40 80 120 160 200
1 2 3 4 5 6 7 8 9 10 11 12 13 14 15 16 17 18 19 20

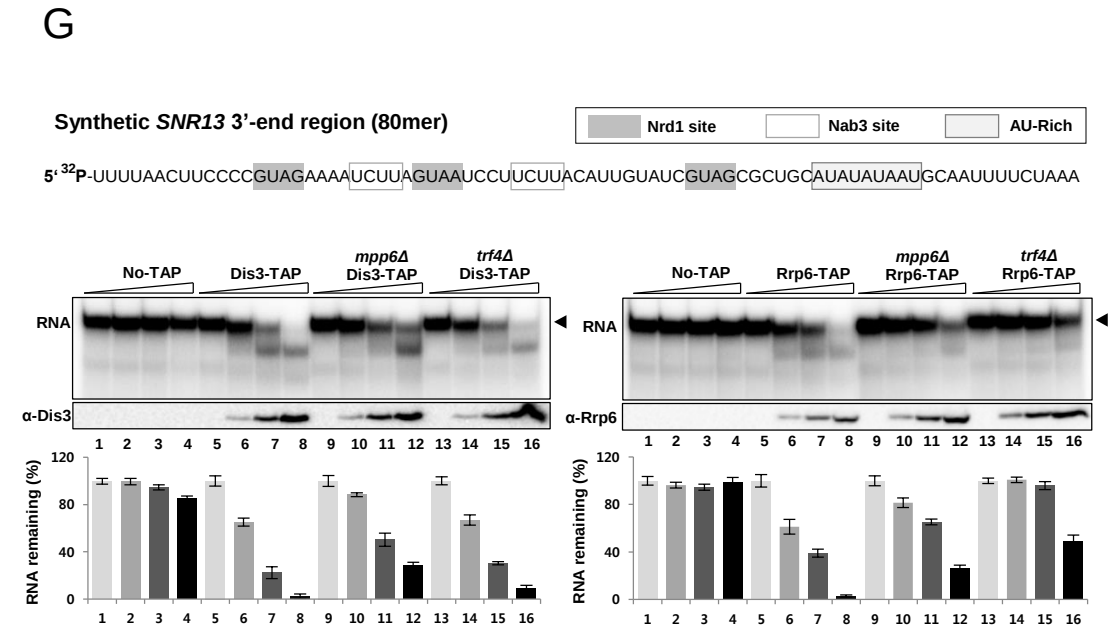
G
Synthetic SNR13 3'-end region (80mer)
Nrd1 site
Nab3 site
AU-Rich
5' 32P-UUUUAACUUCCCCGUAGAAAAUCUUAGUAAUCCUUCUUACAUUGUAUCGUAGCGCUGCAUAUAUAAUGCAAUUUUCUAAA
No-TAP
Dis3-TAP
mpp6Δ Dis3-TAP
trf4Δ Dis3-TAP
RNA
α-Dis3
1 2 3 4 5 6 7 8 9 10 11 12 13 14 15 16
RNA remaining (%)
0 40 80 120
No-TAP
Rrp6-TAP
mpp6Δ Rrp6-TAP
trf4Δ Rrp6-TAP
RNA
α-Rrp6
1 2 3 4 5 6 7 8 9 10 11 12 13 14 15 16
RNA remaining (%)
0 40 80 120

Figure 9. Distinct roles of Mpp6 and Trf4 in 3'-end processing by the exosome.

(**A-C**) Total RNAs were isolated from indicated strains and analyzed by Northern blotting for the *SNR13* and *SNR33* genes. RNAs extracted upon depletion of *RRP6* (A) or *DIS3* (**B**) using the *GAL* promoter, or deletion of *MPP6* and/or *TRF4* (C) were loaded onto 1.5% agarose gel. Pre-snoRNA transcripts are denoted by *black arrowhead*; read-through transcripts by *gray arrowhead*; Gal, growth in galactose; Glu, growth in glucose; ribosomal RNAs are shown as a loading control.

(**D**) Putative RNA processing pathways for the Nrd1-terminated transcripts.

(**E**) RNAs extracted from indicated strains were loaded onto 8% acrylamide gel to separate truncated and mature snoRNAs.

(**F**) The level of pre-snoRNA transcripts relative to mature snoRNAs (set to 100%) is quantified.

(**G**) A synthetic RNA substrate derived from the 3'-end of the *SNR13 gene* was incubated with increasing amounts of Dis3 (left panel) or Rrp6 (right panel) isolated from indicated strains via TAP purification. Its RNA sequence is shown above; amounts of TAP-purified enzymes added in the assay were assessed by western blot; the amounts of remaining RNAs (*black arrowhead*) relative to the initial RNAs with no nuclease added (lanes 1, 5, 9, and 13, set to 100%) are shown

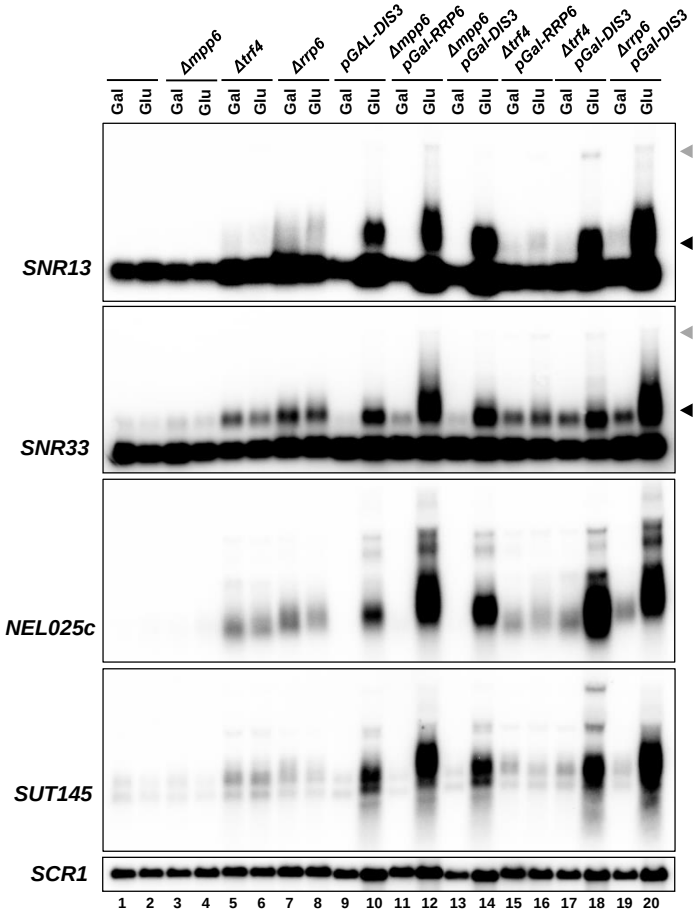

Figure 10. Cumulative RNA processing defects were observed for various non-coding RNAs.

Total RNAs isolated from indicated strains were loaded onto 1.5% agarose gel. Genes analyzed by Northern blot are indicated on left side; pre-snoRNA transcripts are denoted by *black arrowhead*; read-through transcripts are denoted by *gray arrowhead*; Gal, growth in galactose; Glu, growth in glucose; *SCR1* is shown as a loading control.

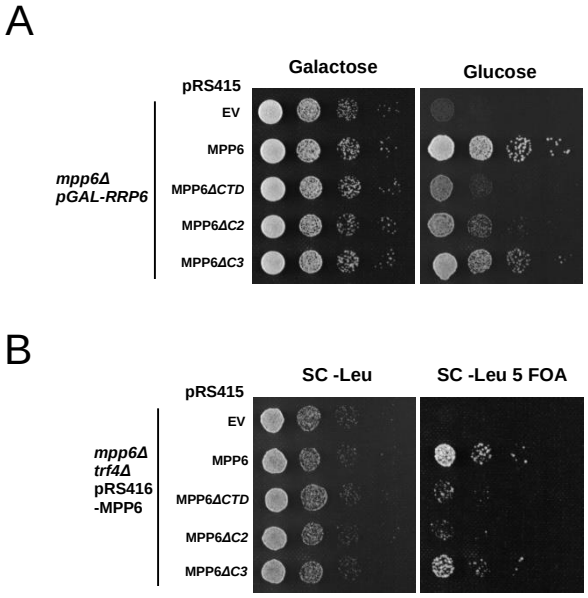

Figure 11. Restoration of the Nrd1-Mpp6 interaction rescues cell growth defect

(**A, B**) Cell growth defect rescues in *mpp6Δ pGAL-RRP6* (A) and *mpp6Δ trf4Δ* (B) strains. But Mpp6 devoid of the C2 region (Nrd1 CID-binding region) does not.

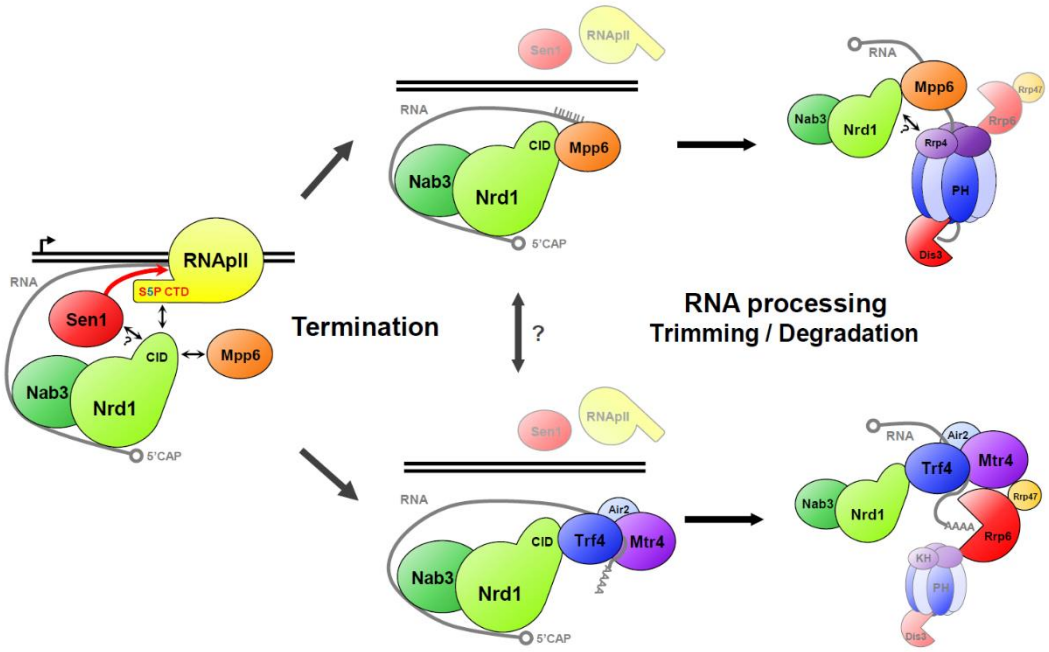

Figure 12. Model for roles of Mpp6 and Trf4 in Nrd1-dependent termination and RNA processing.

The Nrd1 CID binds to early elongating RNApII via Ser5P CTD. By interacting with the CID, Mpp6 may help maintain the Nrd1-Ser5P CTD interaction at an appropriate level and/or to release Nrd1 from the CTD, allowing other factors to bind the CTD. Once RNApII terminates at 3'-ends, the Nrd1 CID is freed from the polymerase, and Mpp6 and Trf4 competitively interact with the CID to set out RNA processing by the exosome. Mpp6 guides the Nrd1-terminated transcripts to Dis3-dependent processing by excluding Trf4 and Rrp6. On the other hand, binding of Trf4 to the Nrd1 CID leads to Rrp6-dependent processing through its interaction with Rrp6 and/or Mtr4. Thus, Mpp6 and Trf4 play key roles in choosing a particular RNA processing route within the exosome. Proteins are not drawn to scale.

DISCUSSION

The CID of Nrd1 contributes to recruiting Nrd1 to early elongating RNApII by recognizing Ser5P CTD of the polymerase (Vasiljeva et al, 2008). Deletion of the CID has a strong impact on Nrd1 recruitment, but also greatly reduces the interaction with Rrp6 and Trf4 (Heo et al, 2013). Thus, the Nrd1 CID couples termination with subsequent RNA processing by recruiting the exosome. However, the molecular basis for this coupling was not clearly understood. In this work, I found that Mpp6 and Trf4 bind to the Nrd1 CID, regulating the interaction of Nrd1 with RNApII and the exosome. Furthermore, these two proteins play pivotal roles in choosing a particular exonucleolytic route within the exosome for the processing of Nrd1-terminated transcripts.

Structural and binding competition experiments demonstrate that RNApII CTD, Mpp6, and Trf4 bind to the Nrd1 CID in a mutually exclusive manner. Unfortunately, I could not detect ChIP signals for Mpp6 and Trf4 on several genes tested, implying that their interactions with Nrd1 may be transient and/or occur off the chromatin after termination. In a simple model, the Nrd1 CID would first bind to Ser5P CTD soon after RNApII begins transcription at 5'-ends of genes, and then be handed over to Mpp6 or Trf4 once RNApII terminates at 3'-ends to set out RNA processing by the exosome. However, deletion of *MPP6* significantly increased Nrd1 recruitment at 5'-ends, suggesting that Mpp6 binds to the CID to compete with Ser5P CTD at 5'-ends as well (**Figure 4 and Figure 5**). Alternatively, deletion of *MPP6* may simply increase and/or free up the pool of Nrd1 off the DNA, thus more Nrd1 would be available to bind early elongating RNApII. In either case, Mpp6 may help maintain the Nrd1-Ser5P CTD interaction at an appropriate level and/or release Nrd1 from the CTD, allowing other factors to bind. By doing so, Mpp6 may indirectly affect RNApII termination by Nrd1. Indeed, I observed increased read-through transcripts in *mpp6Δ* mutant when combined with Rrp6 depletion (**Figure 9A**, lane 8, grey

arrowheads), although these were weaker than those seen in Nrd1ΔCID mutants.

It is unclear why Trf4 does not participate in a competition with Ser5P CTD. Being a part of TRAMP complex that intimately associates with the exosome might temporally and/or sterically prevent Trf4 from competing with Ser5P CTD at 5'-ends. In contrast, if Mpp6 cannot accommodate Nrd1 and Rrp6 at the same time due to a common binding motif (MC-2) (**Figure 1C, D and Figure 6D**), Mpp6 alone could compete with Ser5P CTD to bind the Nrd1 CID.

The association with Nrd1 and subsequent RNA processing by Rrp6 and Dis3 were significantly but differentially affected by deletion of *MPP6* or *TRF4* (**Figure 7 and Fig 9**). These results suggest there are two distinct RNA processing pathways for Nrd1-terminated transcripts (**Figure 12**). Reconstituted exosome complex revealed that RNA degradation route to Rrp6 or Dis3 is randomly chosen (i.e. stochastic) *in vitro* (Wasmuth et al, 2014), but RNAs are often preferentially degraded by one or the other exonuclease *in vivo*, indicating that some exosome-associated factors may affect the route selection. Based upon the results, I propose that Mpp6 and Trf4 play key roles in choosing a particular RNA processing route. When Mpp6 binds to the Nrd1 CID, it would not only preclude Trf4 from interacting with the CID, but it may also block the association between Mpp6 and Rrp6. Thus, Mpp6 could guide the RNAs to Dis3-dependent processing (**Figure 12**). A recent report that Mpp6 directly binds to the core exosome independently of Rrp6 may reflect a role of Mpp6 in Dis3-mediated RNA degradation (Schuch et al, 2014). On the other hand, binding of Trf4 to the Nrd1 CID would exclude Mpp6 and lead to Rrp6-dependent processing of the transcripts via Trf4-Rrp6 and/or Trf4-Mtr4-Rrp6/Rrp47 interactions (Schuch et al, 2014; Tudek et al, 2014). Consistently, deletion of *MPP6* increases the interaction of Nrd1 with Rrp6 (**Figure 7A and C**), and makes the RNA processing of Nrd1-terminated transcripts more dependent upon Rrp6 (**Figure 9A, E and F**).

It would be interesting to uncover how the competition between Mpp6 and Trf4 toward the CID is regulated at 3'-ends. Given that Mpp6 is a RNA-binding protein with a preference for poly(U) and poly(C) but not for poly(A) (Milligan et al, 2008; Schilders et al, 2005), pyrimidine-rich RNA sequences at 3'-ends may favor Mpp6 over Trf4. Another interesting feature that potentially biases the competition might be phosphorylation. According to the phosphoGRID database (http://www.phosphogrid.org), the regions within Mpp6 and Trf4 that interact with the Nrd1 CID contain experimentally verified *in vivo* phosphorylation sites (T148 and S150 in Mpp6, S570 and S571 in Trf4) (Bodenmiller et al, 2010; Soufi et al, 2009). Phosphorylation of these residues might considerably affect the interactions of Mpp6 and Trf4 with Nrd1, as seen for the CTD of RNApII. How the phosphorylation affects the interactions and when it is added and removed remain to be investigated in future studies.

A common binding motif for Nrd1 and Rrp6 within Mpp6 predicts that Mpp6 may be able to associate with Rrp6 independently of Nrd1. It is unclear whether Mpp6 interacts with Rrp6 alone or along with the core exosome and/or TRAMP complex. In either case, Mpp6 might assist Rrp6 to degrade or trim RNA substrates (5.8S rRNA, etc) other than Nrd1-terminated transcripts through interaction with RNA. Considering that Mpp6 binds to the EXO domain of Rrp6 (**Figure 6C and D**), it may facilitate the entry of the RNA substrate into the catalytic center of the enzyme.

MATERIALS AND METHODS

Yeast strains.

Strains used in this study are listed in **Table 2**. For C-terminal 5x myc-tagging, TAP-tag on each protein was switched to 5x myc-tag by transforming the strains with an epitope switching cassette amplified from pFA6a-Myc-KlURA3 (Sung et al, 2008).

Yeast two-hybrid (Y2H) analysis.

The selection strain PJ69-4a (harboring selectable *GAL* UAS-dependent *HIS3* and *ADE2* reporter genes) and improved Gal4 activation domain (GAD, Leu marker) and binding domain (GBD, Trp marker) fusion plasmids were used to identify specific protein-protein interaction, as described previously (James et al, 1996). Transformed cells were plated on SC -Leu -Trp -His to select clones allowing activation of the *HIS3* reporter gene. After growth at 30℃ for 3 days under this low stringency condition, each clone was replica-plated onto SC -Leu -Trp -Ade medium to select transformants that also allow activation of the more stringent *ADE2* reporter. For spotting analysis, cells were grown in SC -Leu -Trp medium for ~16 hr and adjusted to $OD_{600} \approx 0.3$. A small aliquot (~5 μl) from each cell suspension was put on SC -Leu -Trp, -Leu -Trp -His or SC -Leu -Trp -Ade plates.

Cloning, expression, and purification.

The Nrd1 CID (residues 1–154) and the Mpp6 CTD (residues 122–186) were cloned into a modified pET32a vector (Merck Millipore) with N-terminal His_6 and thioredoxin tags and verified by DNA sequencing. The plasmids were introduced into *Escherichia coli* strain BL21star (DE3) (Invitrogen) cells for expression. Transformed cells were grown in LB or minimal medium (with $^{15}NH_4Cl$ and/or $^{13}C_6$-glucose as sole nitrogen or carbon sources,

respectively). Protein expression was induced by 1 mM isopropyl-D-thiogalactopyranoside at an OD_{600} of 0.6~0.8, and the cells were harvested by centrifugation after 5 hr of induction.

For purification of the Nrd1 CID, cell pellets were resuspended in 50 mL (per liter of culture) of lysis buffer I (20 mM Tris, pH 7.4, 200 mM NaCl, 10 mM β-mercaptoethanol, 1 mM phenylmethylsulfonyl fluoride), lysed using Emulsiflex C3 (Avestin, Canada), and centrifuged at 25,000 × g for 20 min. The supernatant fraction was loaded onto HisTrap HP column (GE Healthcare), and the fusion protein was eluted with a 100-ml gradient of imidazole (0–500 mM). It was subsequently dialyzed against buffer D1 (50 mM Tris, pH 8.0, 50 mM NaCl, and 10 mM β-mercaptoethanol), and the His_6 tag was cleaved by TEV protease. Digestion reaction mixture was loaded onto HisTrap column to remove uncleaved proteins. The Nrd1 CID was further purified by size exclusion chromatography using HiLoad Superdex 75 column (GE Healthcare).

For purification of the Mpp6 CTD, cell pellets were resuspended in 50 mL (per liter of culture) of lysis buffer II (20 mM Tris, pH 7.4, 1 M NaCl, 6.3 M urea, 1 mM phenylmethylsulfonyl fluoride), lysed, and centrifuged as in the Nrd1 CID purification. The supernatant fraction was loaded onto HisTrap column (GE Healthcare) and refolded on column using 10 CV of (20 mM Tris, pH 7.4, 200 mM NaCl). After the fusion protein was eluted with a 100-ml gradient of imidazole (10–500 mM) and dialyzed against buffer D1, His_6 tag was cleaved by TEV protease. Digestion reaction mixture was loaded onto HisTrap column. The cleaved Mpp6 CTD was equilibrated with (20 mM Tris, pH 7.4, 100 mM NaCl), loaded onto Mono S column (GE Healthcare), and eluted with a gradient (0.1-1 M NaCl). Fractions containing the target protein were identified by SDS-polyacrylamide gel electrophoresis. For NMR spectroscopy and ITC, all protein samples were further dialyzed against buffer D2 (50 mM sodium phosphate, pH 7.4, 100 mM NaCl, and 10 mM β-mercaptoethanol).

Isothermal titration calorimetry (ITC).

ITC was performed at 25℃ using iTC200 calorimeter (GE Healthcare). The Mpp6 CTD (0.3 mM) in a cell was titrated with 3 mM of the Nrd1 CID, and 0.16 mM of the Trf4 NIM in a cell with 1.6 mM of the Nrd1 CID. Twenty consecutive 2 μl aliquots of protein were titrated into the cell. The duration of each injection was 4 sec, and injections were made at intervals of 150 sec. The heats associated with dilution of the substrates were subtracted from the measured heats of binding. ITC titration data were analyzed with the Origin program (version 7.0).

NMR spectroscopy.

NMR spectra were recorded at 25℃ on Bruker 600 and 800 MHz spectrometers equipped with a *z*-shielded gradient triple resonance probe. The NMR sample contained 1 mM $^{13}C,^{15}N$-Nrd1 CID in buffer D2. Sequential and side chain assignments of ^{1}H, ^{15}N, and ^{13}C resonances were achieved by three-dimensional triple resonance through-bond scalar correlation CBCACONH and HNCACB experiments. For NMR titration, $^{1}H–^{15}N$ HSQC spectra recorded on 0.2 mM of the Nrd1 CID was stoichiometrically titrated with the Mpp6 CTD or the Trf4 NIM, and changes in the backbone amide chemical shifts were monitored. Weighted average chemical shift perturbation was calculated using the equation $\Delta\delta = ([(\Delta\delta_{HN})^2 + (\Delta\delta_N)^2/25]/2)^{1/2}$, and $\Delta\delta$ values larger than 0.1 were selected to represent the binding interfaces.

Chromatin immunoprecipitations (ChIPs).

ChIP procedures and quantification were performed as described (Kim et al, 2004) with oligonucleotides as listed in **Table 3**. ChIPed DNAs were analyzed in real-time using

SYBR Green Supermix and CFX96 cycler (Bio-Rad). Variation between duplicate PCR reactions is less than 5% (as measured by the internal control PCR product) and variation between experiments was typically less than 20%.

Co-immunoprecipitation and western blotting analysis.

Cells were grown in SC medium to an $OD_{600} \approx 1.6$ and broken by glass beads in lysis buffer (20 mM Tris pH 7.6, 100 mM NaCl, 5 mM $MgCl_2$, 1 mM EDTA, 10% glycerol, 0.05% NP-40, 1 mM DTT) supplemented with protease inhibitors and phosphatase inhibitors. About 8 mg of extracts were incubated O/N with IgG sepharose beads (GE healthcare) at 4℃. Pelleted beads were washed three times with ice-cold lysis buffer and boiled for 5 min with 2x SDS loading buffer. After SDS-PAGE, co-IPed proteins were monitored by specific antibodies: 3E8 for CTD Ser5P (Millipore), 9E10 for myc-tagged proteins (Covance), and peroxidase anti-peroxidase for TAP-tagged Nrd1 (SIGMA).

Peptide binding assay using magnetic beads.

Biotinylated-peptides (Ser5P CTD [three repeats] and Trf4 NIM) were bound to streptavidin-coated magnetic beads (Dynabeads MyOne streptavidin T1, Invitrogen) in binding buffer (25 mM Tris pH 7.6, 50 mM NaCl, 1 mM DTT, 5% Glycerol, 0.02% Triton X-100). Beads were then washed with binding buffer to remove unbound peptides. The recombinant Nrd1 CID proteins were incubated in incubation buffer (50 mM Tris pH 7.6, 100 mM NaCl, 1 mM DTT, 5% Glycerol, 0.02% NP-40, 0.02% Triton X-100) for ~16 hr at 4℃ and washed with incubation buffer. Subsequently, increasing amounts of the recombinant Mpp6 protein were added to the beads and further incubated for ~ 8hr at 4℃. After washing with incubation buffer three times, pelleted beads were boiled for 5 min with 2x SDS loading buffer for SDS-PAGE analysis.

Northern blot analysis.

Total RNAs were isolated using hot phenol extraction method and quantified by NanoDrop 2000c (Thermo Scientific). About 45 μg of total RNAs were loaded onto 1.5% MOPS-formaldehyde agarose gel or urea-containing 8% acrylamide gel. RNAs were transferred onto NYTRAN N membrane (Whatman) using capillary method for 20~24 hr, and prehybridization was carried out for 2 hr at 65℃ in prehybridization buffer (300 mM sodium phosphate buffer (pH 7.2), 1% BSA (w/v), 7% SDS, 1 mM EDTA). Hybridization was performed in the same conditions with a radio-labeled probe for ~16 hr, and the membranes were washed in 2X SSC/0.1% SDS and 0.2X SSC/0.1% SDS at RT or 42 ℃. After washes, the membranes were analyzed by phosphoimager (BAS1500, Fuji). Single-strand probes were generated by uni-directional PCR, as previously described (Heo et al, 2013). Briefly, about 5 ng of purified DNA templates (150-250 bp) were assembled with 200 μM each of dGTP, dATP, and dTTP, 5 μM oligo (anti-sense to the RNA being analyzed), 5 μl of [α-^{32}P] dCTP (3,000 Ci/mmol), and Taq DNA polymerase in a total volume of 20 μl. PCR was performed for 40 cycles (94℃, 30 sec; 55℃, 30 sec; 72℃, 50 sec), and unincorporated radio-nucleotide was removed by ProbeQuant G-50 Micro Column (GE Healthcare). The purified probe was denatured by heating at 95℃ for 5 min, chilled on ice, and added into 15 ml hybridization solution. rRNA and *SCR1* were used as a loading control.

pGAL::RRP6 and *pGAL::DIS3* strains were grown on 2% galactose and 1% raffinose medium at 30℃ to an $OD_{600} \approx 0.8$ and shifted to 2% glucose media after washing with sterile water. Cells were then incubated at 30℃ for 12 hr, transferred once again to fresh 2% glucose media, and further incubated for 12 hr (total 24 hr).

RNA degradation assay.

Cells (Dis3-TAP, Rrp6-TAP strains) were grown in SC medium to an $OD_{600} \approx 1.6$ and broken by glass beads in lysis buffer (20 mM Tris pH 7.6, 150 mM NaCl, 5 mM $MgCl_2$, 1 mM EDTA, 10% glycerol, 0.05% NP-40, 1 mM DTT) supplemented with protease inhibitors. About 15 mg of extracts were incubated O/N with IgG sepharose beads (GE healthcare) at 4℃. Pelleted beads were washed three times with ice-cold lysis buffer and TAP tag was cleaved by TEV protease in TEV cleavage buffer (10 mM Tris pH 7.6, 100 mM NaCl, 0.5 mM EDTA) O/N at 4℃.

Synthetic RNA substrate (80 bases) derived from the 3'-end of *SNR13 gene* was 5'-radiolabeled with T4 polynucleotide kinase (NEB, #M0201L) and [γ-^{32}P] ATP (3000 Ci/mmol) at 37℃ for 50 min. Radiolabeling reaction was terminated by incubating at 65℃ for 20 min. Labeled RNA substrate was incubated with increasing amounts of purified proteins in RNA incubation buffer (20 mM Tris pH 7.6, 150 mM NaCl, 5 mM $MgCl_2$, 1 mM DTT) at 30℃ for 30 min. Each reaction mixture was loaded onto urea-containing 10% acrylamide gel and analyzed by phosphoimager (BAS1500, Fuji).

Table 2. Yeast Strains Used in This Study

Strain	Genotype	Source
YF1(BY4741)	MATa, ura3Δ0, leu2Δ0, his3Δ1, met15Δ0	1
YF2	MATa, ura3Δ0, leu2Δ0, his3Δ1, met15Δ0, NRD1-TAP::HIS3	2
YF45	MATa, ura3Δ0, leu2Δ0, his3Δ1, met15Δ0, DIS3-TAP tag::HIS3	2
YF47	MATa, ura3Δ0, leu2Δ0, his3Δ1, met15Δ0, rrp6Δ::KanMX	2
YF57	MATa, ura3Δ0, leu2Δ0, his3Δ1, met15Δ0, RRP6-TAP tag::HIS3	2
YF59/YSB2091	MATa, ura3Δ0, leu2Δ0, his3Δ1, met15Δ0, nrd1Δ6-150-TAP::HIS3	3
YF88	MATa, ura3Δ0, leu2Δ0, his3Δ1, met15Δ0, mpp6Δ::KanMX	2
YF96/YSB2064	MATa, ura3Δ0, leu2Δ0, his3Δ1, met15Δ0, nrd1Δ6-150	3
YF120/pJ69-4A	MATa, ura3-52, leu2-3,112, trp1-901, his3Δ200, gal4Δ, gal80Δ, GAL2-ADE2, LYS2::GAL1-HIS3, met2::GAL7-lacZ, pJ69-4A	4
YF86/YSB2084	MATa, ura3-52, leu2Δ1, trp1Δ63, SEN1-Myc13::KanMX6	5
YMK160	MATa, ura3Δ0, leu2Δ0, his3Δ1, met15Δ0, DIS3-Myc5::KlURA3	5
YMK161	MATa, ura3Δ0, leu2Δ0, his3Δ1, met15Δ0, RRP4-Myc5::KlURA3	5
YMK162	MATa, ura3Δ0, leu2Δ0, his3Δ1, met15Δ0, RRP6-Myc5::KlURA3	5
YMK163	MATa, ura3Δ0, leu2Δ0, his3Δ1, met15Δ0, RRP41-Myc5::KlURA3	5
YMK165	MATa, ura3Δ0, leu2Δ0, his3Δ1, met15Δ0, TRF4-Myc5::KlURA3	5
YMK166	MATa, ura3Δ0, leu2Δ0, his3Δ1, met15Δ0, NRD1-TAP::HIS3, DIS3-Myc5::KlURA3	5
YMK167	MATa, ura3Δ0, leu2Δ0, his3Δ1, met15Δ0, NRD1-TAP::HIS3, RRP4-Myc5::KlURA3	5
YMK168	MATa, ura3Δ0, leu2Δ0, his3Δ1, met15Δ0, NRD1-TAP::HIS3, RRP6-Myc5::KlURA3	5
YMK178	MATa, ura3Δ0, leu2Δ0, his3Δ1, met15Δ0, RTT103-TAP::HIS3, DIS3-Myc5::KlURA3	5
YMK179	MATa, ura3Δ0, leu2Δ0, his3Δ1, met15Δ0, RTT103-TAP::HIS3, RRP4-Myc5::KlURA3	5
YMK180	MATa, ura3Δ0, leu2Δ0, his3Δ1, met15Δ0, RTT103-TAP::HIS3, RRP6-Myc5::KlURA3	5
YMK190	MATa, ura3Δ0, leu2Δ0, his3Δ1, met15Δ0, NRD1-TAP::HIS3, RRP41-Myc5::KlURA3	5
YMK194	MATa, ura3Δ0, leu2Δ0, his3Δ1, met15Δ0, RTT103-TAP::HIS3, RRP41-Myc5::KlURA3	5
YMK196	MATa, ura3Δ0, leu2Δ0, his3Δ1, met15Δ0, nrd1Δ6-150- TAP tag::HIS3, RRP41-Myc5::KlURA3	5
YMK197	MATa, ura3Δ0, leu2Δ0, his3Δ1, met15Δ0, NRD1-TAP::HIS3, TRF4-Myc5::KlURA3	5
YMK201	MATa, ura3Δ0, leu2Δ0, his3Δ1, met15Δ0, RTT103-TAP::HIS3, TRF4-Myc5::KlURA3	5
YMK203	MATa, ura3Δ0, leu2Δ0, his3Δ1, met15Δ0, nrd1Δ6-150- TAP tag::HIS3, TRF4-Myc5::KlURA3	5
YMK204	MATa, ura3Δ0, leu2Δ0, his3Δ1, met15Δ0, nrd1Δ6-150- TAP tag::HIS3, DIS3-Myc5::KlURA3	5
YMK205	MATa, ura3Δ0, leu2Δ0, his3Δ1, met15Δ0, nrd1Δ6-150- TAP tag::HIS3, RRP4-Myc5::KlURA3	5
YMK206	MATa, ura3Δ0, leu2Δ0, his3Δ1, met15Δ0, nrd1Δ6-150- TAP tag::HIS3, RRP6-Myc5::KlURA3	5
YMK215	MATa, ura3Δ0, leu2Δ0, his3Δ1, met15Δ0, RRP47-Myc5::KlURA3	6
YMK233	MATa, ura3Δ0, leu2Δ0, his3Δ1, met15Δ0, MPP6-Myc5::KlURA3	6
YMK238	MATa, ura3Δ0, leu2Δ0, his3Δ1, met15Δ0, NRD1-TAP::HIS3, MPP6-Myc5::KlURA3	6
YMK242	MATa, ura3Δ0, leu2Δ0, his3Δ1, met15Δ0, RTT103- TAP tag::HIS3, MPP6-Myc5::KlURA3	6
YMK244	MATa, ura3Δ0, leu2Δ0, his3Δ1, met15Δ0, nrd1Δ6-150- TAP tag::HIS3, MPP6-Myc5::KlURA3	6
YMK245	MATa, ura3Δ0, leu2Δ0, his3Δ1, met15Δ0, DIS3-Myc5::KlURA3, mpp6Δ::KanMX	6
YMK246	MATa, ura3Δ0, leu2Δ0, his3Δ1, met15Δ0, RRP4-Myc5::KlURA3, mpp6Δ::KanMX	6
YMK247	MATa, ura3Δ0, leu2Δ0, his3Δ1, met15Δ0, RRP6-Myc5::KlURA3, mpp6Δ::KanMX	6
YMK248	MATa, ura3Δ0, leu2Δ0, his3Δ1, met15Δ0, RRP41-Myc5::KlURA3, mpp6Δ::KanMX	6
YMK249	MATa, ura3Δ0, leu2Δ0, his3Δ1, met15Δ0, TRF4-Myc5::KlURA3, mpp6Δ::KanMX	6
YMK250	MATa, ura3Δ0, leu2Δ0, his3Δ1, met15Δ0, NRD1-TAP::HIS3, DIS3-Myc5::KlURA3, mpp6Δ::KanMX	6
YMK251	MATa, ura3Δ0, leu2Δ0, his3Δ1, met15Δ0, NRD1-TAP::HIS3, RRP4-Myc5::KlURA3, mpp6Δ::KanMX	6
YMK252	MATa, ura3Δ0, leu2Δ0, his3Δ1, met15Δ0, NRD1-TAP::HIS3, RRP6-Myc5::KlURA3, mpp6Δ::KanMX	6
YMK253	MATa, ura3Δ0, leu2Δ0, his3Δ1, met15Δ0, NRD1-TAP::HIS3, RRP41-Myc5::KlURA3, mpp6Δ::KanMX	6
YMK254	MATa, ura3Δ0, leu2Δ0, his3Δ1, met15Δ0, NRD1-TAP::HIS3, TRF4-Myc5::KlURA3, mpp6Δ::KanMX	6
YMK263	MATa, ura3Δ0, leu2Δ0, his3Δ1, met15Δ0, NRD1-TAP::HIS3, RRP47-Myc5::KlURA3	6
YMK267	MATa, ura3Δ0, leu2Δ0, his3Δ1, met15Δ0, RTT103-TAP tag::HIS3, RRP47-Myc5::KlURA3	6
YMK269	MATa, ura3Δ0, leu2Δ0, his3Δ1, met15Δ0, nrd1Δ6-150- TAP tag::HIS3, RRP47-Myc5::KlURA3	6
YMK283	MATa, ura3Δ0, leu2Δ0, his3Δ1, met15Δ0, nrd1Δ6-150- TAP tag::HIS3, mpp6Δ::KanMX	6
YMK284	MATa, ura3Δ0, leu2Δ0, his3Δ1, met15Δ0, nrd1Δ6-150 aa, mpp6Δ::KanMX	6
YMK285	MATa, ura3Δ0, leu2Δ0, his3Δ1, met15Δ0, CSL4-Myc5::KlURA3	6
YMK286	MATa, ura3Δ0, leu2Δ0, his3Δ1, met15Δ0, RRP40-Myc5::KlURA3	6
YMK292	MATa, ura3Δ0, leu2Δ0, his3Δ1, met15Δ0, HIS3::pGAL-RRP6	6
YMK293	MATa, ura3Δ0, leu2Δ0, his3Δ1, met15Δ0, mpp6Δ::KanMX, HIS3::pGAL-RRP6	6
YMK294	MATa, ura3Δ0, leu2Δ0, his3Δ1, met15Δ0, nrd1Δ6-150 aa, mpp6Δ::KanMX, HIS3::pGAL-RRP6	6
YMK296	MATa, ura3Δ0, leu2Δ0, his3Δ1, met15Δ0, nrd1Δ6-150 aa, HIS3::pGAL-RRP6	6
YMK297	MATa, ura3Δ0, leu2Δ0, his3Δ1, met15Δ0, NRD1-TAP::HIS3, RRP40-Myc5::KlURA3	6
YMK299	MATa, ura3Δ0, leu2Δ0, his3Δ1, met15Δ0, RTT103-TAP tag::HIS3, RRP40-Myc5::KlURA3	6
YMK300	MATa, ura3Δ0, leu2Δ0, his3Δ1, met15Δ0, nrd1Δ6-150- TAP tag::HIS3, RRP40-Myc5::KlURA3	6

YMK305	MATa, ura3Δ0, leu2Δ0, his3Δ1, met15Δ0, NRD1-TAP::HIS3, CSL4-Myc5::KlURA3	6
YMK307	MATa, ura3Δ0, leu2Δ0, his3Δ1, met15Δ0, RTT103-TAP tag::HIS3, CSL4-Myc5::KlURA3	6
YMK308	MATa, ura3Δ0, leu2Δ0, his3Δ1, met15Δ0, nrd1Δ6-150- TAP tag::HIS3, CSL4-Myc5::KlURA3	6
YMK319	MATa, ura3Δ0, leu2Δ0, his3Δ1, met15Δ0, NRD1-TAP::HIS3, trf4Δ::KanMX	6
YMK320	MATa, ura3Δ0, leu2Δ0, his3Δ1, met15Δ0, nrd1Δ6-150- TAP tag::HIS3, trf4Δ::KanMX	6
YMK322	MATa, ura3Δ0, leu2Δ0, his3Δ1, met15Δ0, trf4Δ::KanMX, mpp6Δ::HPH, pRS416-MPP6	6
YMK324	MATa, ura3Δ0, leu2Δ0, his3Δ1, met15Δ0, RRP6-TAP tag::HIS3, mpp6Δ::KanMX	6
YMK325	MATa, ura3Δ0, leu2Δ0, his3Δ1, met15Δ0, RRP6-TAP tag::HIS3, trf4Δ::KanMX	6
YMK326	MATa, ura3Δ0, leu2Δ0, his3Δ1, met15Δ0, trf4Δ::KanMX, RRP6-Myc5::KlURA3	6
YMK327	MATa, ura3Δ0, leu2Δ0, his3Δ1, met15Δ0, NRD1-TAP::HIS3, trf4Δ::KanMX, RRP6-Myc5::KlURA3	6
YMK328	MATa, ura3Δ0, leu2Δ0, his3Δ1, met15Δ0, trf4Δ::KanMX, MPP6-Myc5::KlURA3	6
YMK334	MATa, ura3Δ0, leu2Δ0, his3Δ1, met15Δ0, NRD1-TAP::HIS3, trf4Δ::KanMX, MPP6-Myc5::KlURA3	6
YMK335	MATa, ura3Δ0, leu2Δ0, his3Δ1, met15Δ0, NRD1-TAP::HIS3, mpp6Δ::KanMX	6
YMK422	MATa, ura3Δ0, leu2Δ0, his3Δ1, met15Δ0, SEN1-Myc5::KlURA3	6
YMK423	MATa, ura3Δ0, leu2Δ0, his3Δ1, met15Δ0, nrd1Δ6-150-TAP tag::HIS3, SEN1-Myc13::KanMX	6
YMK424	MATa, ura3Δ0, leu2Δ0, his3Δ1, met15Δ0, RTT103-TAP tag::HIS3, SEN1-Myc13::KanMX	6
YMK425	MATa, ura3Δ0, leu2Δ0, his3Δ1, met15Δ0, mpp6Δ::KanMX, SEN1-Myc5::KlURA3	6
YMK426	MATa, ura3Δ0, leu2Δ0, his3Δ1, met15Δ0, NRD1-TAP tag::HIS3, mpp6Δ::KanMX, SEN1-Myc5::KlURA3	6
YMK427	MATa, ura3Δ0, leu2Δ0, his3Δ1, met15Δ0, trf4Δ::KanMX, SEN1-Myc5::KlURA3	6
YMK428	MATa, ura3Δ0, leu2Δ0, his3Δ1, met15Δ0, NRD1-TAP tag::HIS3, trf4Δ::KanMX, SEN1-Myc5::KlURA3	6
YMK429	MATa, ura3Δ0, leu2Δ0, his3Δ1, met15Δ0, NRD1-TAP tag::HIS3, SEN1-Myc5::KlURA3	6
YMK430	MATa, ura3Δ0, leu2Δ0, his3Δ1, met15Δ0, HIS3::pGAL-DIS3	6
YMK431	MATa, ura3Δ0, leu2Δ0, his3Δ1, met15Δ0, mpp6Δ::KanMX, HIS3::pGAL-DIS3	6
YMK432	MATa, ura3Δ0, leu2Δ0, his3Δ1, met15Δ0, trf4Δ::KanMX, HIS3::pGAL-DIS3	6
YMK433	MATa, ura3Δ0, leu2Δ0, his3Δ1, met15Δ0, nrd1Δ6-150aa, HIS3::pGAL-DIS3	6
YMK434	MATa, ura3Δ0, leu2Δ0, his3Δ1, met15Δ0, nrd1Δ6-150aa, mpp6Δ::KanMX, HIS3::pGAL-DIS3	6
YMK435	MATa, ura3Δ0, leu2Δ0, his3Δ1, met15Δ0, trf4Δ::KanMX, HIS3::pGAL-RRP6	6
YMK436	MATa, ura3Δ0, leu2Δ0, his3Δ1, met15Δ0, rrp6Δ::KanMX, HIS3::pGAL-DIS3	6
YMK437	MATa, ura3Δ0, leu2Δ0, his3Δ1, met15Δ0, trf4Δ::KanMX, DIS3-Myc5::KlURA3	6
YMK438	MATa, ura3Δ0, leu2Δ0, his3Δ1, met15Δ0, NRD1-TAP tag::HIS3, trf4Δ::KanMX, DIS3-Myc5::KlURA3	6
YMK442	MATa, ura3Δ0, leu2Δ0, his3Δ1, met15Δ0, DIS3-TAP tag::HIS3, mpp6Δ::KanMX	6
YMK443	MATa, ura3Δ0, leu2Δ0, his3Δ1, met15Δ0, DIS3-TAP tag::HIS3, trf4Δ::KanMX	6
YMK444	MATa, ura3Δ0, leu2Δ0, his3Δ1, met15Δ0, mpp6Δ::KanMX, pRS315-MPP6-HA3	6
YMK445	MATa, ura3Δ0, leu2Δ0, his3Δ1, met15Δ0, NRD1-TAP tag::HIS3, mpp6Δ::KanMX, pRS315-MPP6-HA3	6
YMK446	MATa, ura3Δ0, leu2Δ0, his3Δ1, met15Δ0, NRD1-TAP tag::HIS3, mpp6Δ::KanMX, pRS315-MPP6ΔC2-HA3	6
YMK447	MATa, ura3Δ0, leu2Δ0, his3Δ1, met15Δ0, mpp6Δ::KanMX, HIS3::pGAL-RRP6, pRS415	6
YMK448	MATa, ura3Δ0, leu2Δ0, his3Δ1, met15Δ0, mpp6Δ::KanMX, HIS3::pGAL-RRP6, pRS415-MPP6	6
YMK449	MATa, ura3Δ0, leu2Δ0, his3Δ1, met15Δ0, mpp6Δ::KanMX, HIS3::pGAL-RRP6, pRS415-MPP6ΔCTD	6
YMK450	MATa, ura3Δ0, leu2Δ0, his3Δ1, met15Δ0, mpp6Δ::KanMX, HIS3::pGAL-RRP6, pRS415-MPP6ΔC2	6
YMK451	MATa, ura3Δ0, leu2Δ0, his3Δ1, met15Δ0, mpp6Δ::KanMX, HIS3::pGAL-RRP6, pRS415-MPP6ΔC3	6
YMK452	MATa, ura3Δ0, leu2Δ0, his3Δ1, met15Δ0, trf4Δ::KanMX, mpp6Δ::HPH, pRS416-MPP6, pRS415	6
YMK453	MATa, ura3Δ0, leu2Δ0, his3Δ1, met15Δ0, trf4Δ::KanMX, mpp6Δ::HPH, pRS416-MPP6, pRS415-MPP6	6
YMK454	MATa, ura3Δ0, leu2Δ0, his3Δ1, met15Δ0, trf4Δ::KanMX, mpp6Δ::HPH, pRS416-MPP6, pRS415-MPP6ΔCTD	6
YMK455	MATa, ura3Δ0, leu2Δ0, his3Δ1, met15Δ0, trf4Δ::KanMX, mpp6Δ::HPH, pRS416-MPP6, pRS415-MPP6ΔC2	6
YMK456	MATa, ura3Δ0, leu2Δ0, his3Δ1, met15Δ0, trf4Δ::KanMX, mpp6Δ::HPH, pRS416-MPP6, pRS415-MPP6ΔC3	6
Total	**104 strains**	

1. Winzeler *et al.* (1999) *Science* 285: 901-906
2. Ghaemmaghami *et al.* (2003) *Nature* 425: 737-741
3. Vasiljeva *et al.* (2008) *Nat. Struc. Mol Biol* 15: 795-804
4. Phillip James *et al.* (1996) *Genetics* 144: 1425
5. Heo *et al.* (2013) *J. Biol. Chem.* 288: 36676-90
6. This study

Table 3. ChIP Oligonucleotides Used in This Study

Oligo #	Name	Sequence
11	TEL (VI)-up	GCGTAACAAAGCCATAATGCCTCC
12	TEL (VI)-low	CTCGTTAGGATCACGTTCGAATCC
18	PMA1 #1-up (-304)	CAAATGTCCTATCATTATCGTCTAAC
19	PMA1 #1-low (-47)	CAATGATTTTCTTTAACTAGCTG
52	PMA1 #2-up (+168)	CGACGACGAAGACAGTGATAACG
53	PMA1 #2-low (+376)	ATTGAATTGGACCGACGAAAAACATAAC
54	PMA1 #3-up (+584)	AAGTCGTCCCAGGTGATATTTTGCA
55	PMA1 #3-low (+807)	AACGAAAGTGTTGTCACCGGTAGC
56	PMA1 #4-up (+1010)	GTTTGCCAGCTGTCGTTACCACCAC
57	PMA1 #4-low (+1250)	TTCTTCTTTCTGGAAGCAGCCAAAC
58	PMA1 #5-up (+2018)	CTATTATTGATGCTTTGAAGACCTCCAG
59	PMA1 #5-low (+2290)	TGCCCAAAATAATAGACATACCCCATAA
60	PMA1 #6-up (+2866)	GATACACTAAAAAGAATTAGGAGCCAAC
61	PMA1 #6-low (+3098)	CAAGAAAGAAAAAGTACCATCCAGAG
62	PMA1 #7-up (+3287)	GAAAATATTTGGTATCTTTGCAAGATG
63	PMA1 #7-low (+3500)	GTAAATTTGTATACGTTCATGTAAGTG
64	PMA1 #8-up (+3448)	GCGCCCATACAGACACTCAAGATAC
65	PMA1 #8-low (+3652)	GGCCTGGCGATTTGTTTGCTTTCTTG
66	PMA1 #9-up (+3745)	ACTACCCTGGCGCTATGATG
67	PMA1 #9-low (+3913)	GGAAACAGCGTGATGAGTGA
68	PMA1 #10-up (+4129)	GTTCATGAAGTCACCTCTCCACAAG
69	PMA1 #10-low (+4353)	CATACCGAAATATGGAACGCCGAACTG
70	PMA1 #11-up (+5300)	CTGATATTTTGGATGCCTATGAACG
71	PMA1 #11-low (+5562)	GTCTTCGGGTTGGACAGGTTCAG
72	snR13 #1-up (-60)	TTATAAATGGCATCTCAAATCGTC
73	snR13 #1-low (+124)	GGTCAGATAAAAGTAAAAAAAGGTAGC
74	snR13 #2-up (+119)	CTGACCTTTTAACTTCCCCGTAG
75	snR13 #2-low (+358)	CTGTCGCTTCCGTGTCTCTTGTCCTG
76	snR13 #3-up (+345)	CACGGAAGCGACAGAAAGACAGGGAG
77	snR13 #3-low (+537)	CTAGAGGGAATGTATGTTGTTGAAG
78	snR13 #4-up (+747)	GAGCATCTGCTTTCCTTTCAC
79	snR13 #4-low (+922)	ATCACGGCGCCTCATCTTTG
80	snR13 #5-up (+1284)	AAAACCAAGAAAAGGATAAAGAG
81	snR13 #5-low (+1524)	TCGGTGTCTACAAAATGATACGC
868	NRD1 #1-up (-189)	TCTTCTTACAATTAGTTACGTTACCG
869	NRD1 #1-low (-35)	CCTTTCCTGTAACTCGTGCTTGG
870	NRD1 #2-up (+107)	CACTTGATCACATTGATATTGAATCG
871	NRD1 #2-low (+248)	TTTGATCTTGTTTCATCCAAGTAAGC
872	NRD1 #3-up (+501)	ACTGGATCCCAAGCAGAGGTCG
873	NRD1 #3-low (+640)	CTATTACTTGGAAAAGAGCTGCTTGC
874	NRD1 #4-up (+1036)	GTACCACTAAACATGAAGGAATGGG
875	NRD1 #4-low (+1198)	GGCTCCATCTTTATTGAAGTTTTGC
876	NRD1 #5-up (+1333)	GGCACTTCTGGTCAACCTCTCG
877	NRD1 #5-low (+1478)	TTGTTAGGTTTACCAGAACGTGGC

REFERENCES

Allmang C, Mitchell P, Petfalski E, Tollervey D (2000) Degradation of ribosomal RNA precursors by the exosome. *Nucleic acids research* **28:** 1684-1691

Arigo JT, Carroll KL, Ames JM, Corden JL (2006a) Regulation of yeast NRD1 expression by premature transcription termination. *Molecular cell* **21:** 641-651

Arigo JT, Eyler DE, Carroll KL, Corden JL (2006b) Termination of cryptic unstable transcripts is directed by yeast RNA-binding proteins Nrd1 and Nab3. *Molecular cell* **23:** 841-851

Bodenmiller B, Wanka S, Kraft C, Urban J, Campbell D, Pedrioli PG, Gerrits B, Picotti P, Lam H, Vitek O, Brusniak MY, Roschitzki B, Zhang C, Shokat KM, Schlapbach R, Colman-Lerner A, Nolan GP, Nesvizhskii AI, Peter M, Loewith R, von Mering C, Aebersold R (2010) Phosphoproteomic analysis reveals interconnected system-wide responses to perturbations of kinases and phosphatases in yeast. *Science signaling* **3:** rs4

Buratowski S (2009) Progression through the RNA polymerase II CTD cycle. *Molecular cell* **36:** 541-546

Butler JS (2002) The yin and yang of the exosome. *Trends in cell biology* **12:** 90-96

Callahan KP, Butler JS (2008) Evidence for core exosome independent function of the nuclear exoribonuclease Rrp6p. *Nucleic acids research* **36:** 6645-6655

Chinchilla K, Rodriguez-Molina JB, Ursic D, Finkel JS, Ansari AZ, Culbertson MR (2012) Interactions of Sen1, Nrd1, and Nab3 with multiple phosphorylated forms of the Rpb1 C-terminal domain in Saccharomyces cerevisiae. *Eukaryotic cell* **11:** 417-429

Heo DH, Yoo I, Kong J, Lidschreiber M, Mayer A, Choi BY, Hahn Y, Cramer P, Buratowski S, Kim M (2013) The RNA polymerase II C-terminal domain-interacting domain of yeast Nrd1 contributes to the choice of termination pathway and couples to RNA processing by

the nuclear exosome. *The Journal of biological chemistry* **288:** 36676-36690

Houseley J, Tollervey D (2009) The many pathways of RNA degradation. *Cell* **136:** 763-776

James P, Halladay J, Craig EA (1996) Genomic libraries and a host strain designed for highly efficient two-hybrid selection in yeast. *Genetics* **144:** 1425-1436

Kim M, Ahn SH, Krogan NJ, Greenblatt JF, Buratowski S (2004) Transitions in RNA polymerase II elongation complexes at the 3' ends of genes. *The EMBO journal* **23:** 354-364

Kim M, Vasiljeva L, Rando OJ, Zhelkovsky A, Moore C, Buratowski S (2006) Distinct pathways for snoRNA and mRNA termination. *Molecular cell* **24:** 723-734

Lehner B, Sanderson CM (2004) A protein interaction framework for human mRNA degradation. *Genome research* **14:** 1315-1323

Liu Q, Greimann JC, Lima CD (2006) Reconstitution, activities, and structure of the eukaryotic RNA exosome. *Cell* **127:** 1223-1237

Lykke-Andersen S, Brodersen DE, Jensen TH (2009) Origins and activities of the eukaryotic exosome. *Journal of cell science* **122:** 1487-1494

Milligan L, Decourty L, Saveanu C, Rappsilber J, Ceulemans H, Jacquier A, Tollervey D (2008) A yeast exosome cofactor, Mpp6, functions in RNA surveillance and in the degradation of noncoding RNA transcripts. *Molecular and cellular biology* **28:** 5446-5457

Mitchell P, Petfalski E, Houalla R, Podtelejnikov A, Mann M, Tollervey D (2003) Rrp47p is an exosome-associated protein required for the 3' processing of stable RNAs. *Molecular and cellular biology* **23:** 6982-6992

Porrua O, Libri D (2013) A bacterial-like mechanism for transcription termination by the Sen1p helicase in budding yeast. *Nature structural & molecular biology* **20:** 884-891

Schilders G, Raijmakers R, Raats JM, Pruijn GJ (2005) MPP6 is an exosome-associated RNA-binding protein involved in 5.8S rRNA maturation. *Nucleic acids research* **33:** 6795-6804

Schilders G, van Dijk E, Pruijn GJ (2007) C1D and hMtr4p associate with the human exosome subunit PM/Scl-100 and are involved in pre-rRNA processing. *Nucleic acids research* **35:** 2564-2572

Schneider C, Tollervey D (2013) Threading the barrel of the RNA exosome. *Trends in biochemical sciences* **38:** 485-493

Schuch B, Feigenbutz M, Makino DL, Falk S, Basquin C, Mitchell P, Conti E (2014) The exosome-binding factors Rrp6 and Rrp47 form a composite surface for recruiting the Mtr4 helicase. *The EMBO journal* **33:** 2829-2846

Soufi B, Kelstrup CD, Stoehr G, Frohlich F, Walther TC, Olsen JV (2009) Global analysis of the yeast osmotic stress response by quantitative proteomics. *Molecular bioSystems* **5:** 1337-1346

Stead JA, Costello JL, Livingstone MJ, Mitchell P (2007) The PMC2NT domain of the catalytic exosome subunit Rrp6p provides the interface for binding with its cofactor Rrp47p, a nucleic acid-binding protein. *Nucleic acids research* **35:** 5556-5567

Steinmetz EJ, Conrad NK, Brow DA, Corden JL (2001) RNA-binding protein Nrd1 directs poly(A)-independent 3'-end formation of RNA polymerase II transcripts. *Nature* **413:** 327-331

Sung MK, Ha CW, Huh WK (2008) A vector system for efficient and economical switching of C-terminal epitope tags in Saccharomyces cerevisiae. *Yeast* **25:** 301-311

Thiebaut M, Kisseleva-Romanova E, Rougemaille M, Boulay J, Libri D (2006) Transcription termination and nuclear degradation of cryptic unstable transcripts: a role for the nrd1-nab3 pathway in genome surveillance. *Molecular cell* **23:** 853-864

Tudek A, Porrua O, Kabzinski T, Lidschreiber M, Kubicek K, Fortova A, Lacroute F, Vanacova S, Cramer P, Stefl R, Libri D (2014) Molecular basis for coordinating transcription termination with noncoding RNA degradation. *Molecular cell* **55:** 467-481

van Hoof A, Lennertz P, Parker R (2000) Yeast exosome mutants accumulate 3'-extended polyadenylated forms of U4 small nuclear RNA and small nucleolar RNAs. *Molecular and cellular biology* **20:** 441-452

Vanacova S, Wolf J, Martin G, Blank D, Dettwiler S, Friedlein A, Langen H, Keith G, Keller W (2005) A new yeast poly(A) polymerase complex involved in RNA quality control. *PLoS biology* **3:** e189

Vasiljeva L, Buratowski S (2006) Nrd1 interacts with the nuclear exosome for 3' processing of RNA polymerase II transcripts. *Molecular cell* **21:** 239-248

Vasiljeva L, Kim M, Mutschler H, Buratowski S, Meinhart A (2008) The Nrd1-Nab3-Sen1 termination complex interacts with the Ser5-phosphorylated RNA polymerase II C-terminal domain. *Nature structural & molecular biology* **15:** 795-804

Wasmuth EV, Januszyk K, Lima CD (2014) Structure of an Rrp6-RNA exosome complex bound to poly(A) RNA. *Nature* **511:** 435-439

Wyers F, Rougemaille M, Badis G, Rousselle JC, Dufour ME, Boulay J, Regnault B, Devaux F, Namane A, Seraphin B, Libri D, Jacquier A (2005) Cryptic pol II transcripts are degraded by a nuclear quality control pathway involving a new poly(A) polymerase. *Cell* **121:** 725-737

ABSTRACT IN KOREAN

국문초록

효모 saccharomyces cerevisiae 의 Nrd1 은 RNA 중합효소 II (RNApII)의 Carboxyl-말단지역 (CTD)을 CTD-Interacting Domain (CID)을 통해 인식하게 되고, nuclear exosome 을 불러 들임으로써 전사종결과 RNA 가공을 하는 역할을 한다. 최근의 보고에 의하면, Nrd1 CID 가 RNApII 종결과 함께 nuclear exosome 을 Nrd1 으로 불러들여 RNA 가공처리 역할을 한다고 알려졌다. 하지만 어떤 단백질이 Nrd1 CID 를 nuclear exosome 으로 연결 시키는지에 대한 것은 불명확 했다. 이번 연구에서는 yeast two hybrid 를 이용하여, Nrd1 CID 와 상호작용하는 nuclear exosome 관련 요소들을 조사하였고, 그 중에 nuclear exosome 보조인자로 알려진 Mpp6 와 Trf4 가 직접적으로 Nrd1 CID 와 결합하는 것을 확인하였다. Mpp6 와 Trf4 는 모두 Nrd1 CID 의 유사한 위치에 결합 하였고, 이는 RNApII CTD 가 결합한다고 알려진 지역과도 상당히 비슷하다는 것을 살펴 볼 수 있었다. 이를 통해 다양한 단백질 (Mpp6, Trf4, RNApII CTD)이 경쟁적으로 상호작용하여 Nrd1 CID 와 결합하면서 일련의 과정들이 진행된다는 것을 살펴 볼 수 있었다. 또한, 다양한 분자생물학 기법의 실험을 통해 Nrd1 에 의해 전사종결 된 RNA 는 Mpp6 를 통해 Dis3 라는 RNA 분해효소로 처리되는 방법과 Trf4 를 이용해 Rrp6 라는 또 다른 RNA 분해효소에 의해 가공처리 되는 구별된 방법이 있다는 것을 알 수 있었다. 결과적으로 nuclear exsome 보조인자인 Mpp6 와 Trf4 가 Nrd1 과 결합함으로써 전사종결 후에 남게 되는 특정 RNA 를 적절한 방법으로 선택하여 가공 처리한다는 것을 발견하였다.

주요어: Nrd1, Mpp6, RNA 중합효소 II, 전사종결, RNA 가공

학번: 2013-22449